ROCK MELT BOREHOLE SEALING SYSTEM
Final Technical Report for
SBIR Phase I Grant No. DE-SC0011888

Principal Investigator
John D. Osnes, Ph.D.

Report No. DOE-RESPEC-0011888
(RESPEC Report RSI-2508)

prepared for

Department of Energy
Office of Science
9800 South Cass Avenue
Argonne, Illinois 60439

March 19, 2015

RESPEC

ROCK MELT BOREHOLE SEALING SYSTEM
Final Technical Report for
SBIR Phase I Grant No. DE-SC0011888

Report No. DOE-RESPEC-0011888
(RESPEC Report RSI-2508)

by

John D. Osnes, Ph.D.
(Principal Investigator)
Cody A. Vining
Jay R. Nopola
RE/SPEC Inc.
3824 Jet Drive
Rapid City, South Dakota 57703

and

William M. Roggenthen, Ph.D.
South Dakota School of Mines & Technology
501 E. St. Joseph Street
Rapid City, South Dakota 57701

prepared for

Department of Energy
Office of Science
9800 South Cass Avenue
Argonne, Illinois 60439

March 19, 2015

EXECUTIVE SUMMARY

Deep borehole disposal is one option that has received attention in recent years as a possible strategy for long-term disposal of the tens of thousands of tons of spent nuclear fuel. The feasibility of the deep borehole option relies upon designing and constructing an effective seal within the borehole that ensures the waste package does not communicate with the shallow subsurface biosphere through the borehole itself. Some of the uncertainty associated with the long-term suitability of the deep borehole option is related to (1) the degradation of traditional sealing materials over time and (2) the inability of traditional sealing methods to adequately seal a Disturbed Rock Zone (DRZ) surrounding the borehole. One possible system to address these concerns consists of melting crushed rock to form a plug in the borehole above the waste package.

OBJECTIVE OF CURRENT STUDY

The current project expands on previous work to further the advancement of the deep borehole disposal concept. The overarching objective of the current study is to evaluate the feasibility of constructing a downhole heater that is capable of meeting the technical and logistical requirements to melt rock. This ultimate objective was accomplished by two primary approaches. The first approach was to define the heater requirements and conceptually design a system that is capable of melting rock. The second approach was to determine the feasibility of conducting an in situ, field-scale melting experiment, which will be necessary to validate the suitability of the rock melt seal. Several requirements must be defined for the successful conceptual design of a rock melt sealing system. The primary questions regarding heater design that this feasibility study attempted to answer include the following:

- What are the power and time requirements for a downhole rock melt heater and is this power requirement still adequate when some of the other material variables are changed?
- What is a reasonable range of thermal properties and melting points that could be encountered in a deep borehole, and how might these properties affect the heater requirements?
- Are “off-the-shelf” products (i.e., resistive-heating elements) available that can be used to provide the preferred power output and withstand the expected downhole conditions (e.g., sustained, high temperatures)?
- How might a conceptual heater be delivered downhole and supplied with power?

The objective of the proposed field-scale melt experiment is to address several key questions that relate to the functionality and integrity of the rock melt concept for sealing the borehole for the deep borehole disposal; specifically:

- What degree of confidence can be placed in achieving a melt plug seal?
- Is the DRZ effectively eliminated through the melting and recrystallization process?
- How effective is the bond between the melt plug and the country rock?

RESULTS OF THE CURRENT STUDY

This study evaluated the feasibility of constructing a downhole heater that is capable of meeting the technical and logistical requirements to melt rock. The evaluation and conceptual design of the heater system resulted in the following primary findings:

- Borehole wall temperatures capable of producing a partial melt are achievable under most expected thermal conductivities with a 12 kilowatt (kW) heater. However, rock with unusually high thermal conductivity (e.g., pure quartz) is able to transport the heat away from the borehole before melting temperatures can be achieved, regardless of time.
- Expected porosity of the backfill should not impact the ability to achieve partial melting temperatures in the host rock, but greater backfill porosities may influence the operation of the heater because temperatures greater than 2,000°C may exceed the temperature rating of conventional heater components.
- Uncertainty in latent heat values had a minimal impact on the temperature distribution around the borehole. Borehole wall temperatures exceeding 800°C were predicted shortly after 36 hours for latent heat values of 271,000 Joules per kilogram (J/kg), 300,000 J/kg, and 419,000 J/kg.
- Commercially available components have been identified that meet the requirements of the heater system, including resistive elements that are capable of providing the required heat generation, container materials that can withstand the anticipated temperatures, and a system capable of providing power to the heater.

The feasibility of performing field-scale experiments in the Sanford Underground Research Facility (SURF) was also evaluated as part of this study and resulted in the following major findings:

- A suitable test location has been identified at SURF. This location will allow in situ testing of the rock melt sealing system in rhyolite dikes (the fine-grained equivalent of granite). The technical and logistical requirements for performing the rock melt tests can be met by using or expanding the existing infrastructure at SURF with on-site personnel (e.g., blasting) and contractors (e.g., drilling).
- Instrumentation of the field-scale tests (e.g. temperature, strain, and pressure measurements) could provide meaningful data with regards to the response of the host rock.

- In situ hydraulic conductivity tests using packers can test the effectiveness of the rock melt seal. Careful drilling and test siting will allow a mine back to be performed from a lower level so that the recrystallized melt can retrieved and further evaluated in a laboratory.
- The preliminary cost estimates for the proposed field-scale tests indicate that a field-scale melting experiment is feasible within a Phase II Small Business Innovation Research (SBIR) budget.

CONCLUSIONS OF THE STUDY

In summary, the rock melt sealing concept has the potential to reduce uncertainty associated with a significant issue facing the nation: the long-term storage of nuclear waste. Preliminary efforts defined the requirements of a downhole heater system that is capable of melting rock. Researching currently available heater components and commercially available refractory metals indicates that developing such a system is feasible using available technology. The next logical step is designing and manufacturing prototype heaters. Concurrent with prototype heater development is coordinating robust field-scale experiments that are capable of validating the design for potential users. The Sanford Underground Research Facility (an underground research laboratory) has been identified as a host site for field testing of prototype heaters. Preliminary costing indicates that a field-scale melting experiment at SURF is feasible within a Phase II SBIR budget while allowing sufficient funding to refine the heater design, coordinate the test program, and interpret the results.

TABLE OF CONTENTS

TABLE OF CONTENTS
(Continued)

LIST OF TABLES

LIST OF FIGURES

LIST OF FIGURES
(Continued)

1.0 INTRODUCTION

The Blue Ribbon Commission (BRC) on America's Nuclear Future Report to the Secretary of Energy [2012] identified the urgent need for the U.S. to develop a new strategy for long-term disposal of the tens of thousands of tons of spent nuclear fuel currently housed at dozens of locations across the nation that are not designed for long-term storage. The BRC concluded that deep geological disposal is the most promising and widely accepted method currently available for long-term disposal of nuclear waste. Deep borehole disposal is one of the options of deep geological disposal that has received attention in recent years because numerous factors suggest it is an inherently safe method of disposal [Arnold et al., 2011; 2013]. The deep borehole concept is currently envisioned as a large-diameter borehole which is 0.91-meter (m) (36-inch) diameter at the surface and telescopes down to approximately 0.43-m (17-inch) diameter at depth for nuclear waste disposal [Arnold et al., 2011]. The target disposal interval for the deep borehole option is crystalline rock, which occurs at depths between 3 kilometers (km) and 5 km. It is envisioned that a borehole will extend at least 3 km into the crystalline bedrock and that the lower 2 km will be used as the waste package disposal zone.

The feasibility of the deep borehole option relies upon designing and constructing an effective seal within the borehole that ensures the waste package does not communicate with the shallow subsurface biosphere through the borehole itself. This requires that the seal subsystem be reliable and long-lasting without substantial degradation over thousands of years. As indicated in the generalized deep borehole concept shown in Figure 1-1, many established sealing options are available for use in the actual borehole, including concrete, bentonite, and asphalt. Although this redundant system of multiple seals consisting of alternating layers of cement and bentonite is based upon standard accepted practices, the long-term performance of materials such as cement and bentonite is still uncertain. Concerns include the mechanical and chemical stability of these components over long periods of time and the effect of high temperatures and corrosive environments on the sealing subsystem. Additionally, a Disturbed Rock Zone (DRZ) will develop and surround the borehole because of drilling damage and the resulting stress differences created by the borehole opening. The DRZ consists of a damaged zone where microfractures (which are disseminated throughout the rock mass) and macrofractures (which are essentially microfractures that have coalesced into visible features) increase the permeability of the crystalline rock surrounding the borehole. The ability of standard techniques to effectively seal the DRZ is also uncertain.

An innovative system for sealing has been proposed by Attrill and Gibb [2003a; 2003b] that considers encapsulating the waste in a melt generated from either the waste itself or a plug above the waste. Subsequent studies addressed issues such as waste package stabilization through backfill materials [Gibb et al., 2008a] and quantitative models for heat generation in deep boreholes [Gibb et al., 2008b], as well as temperature distributions for different geometries of waste in such boreholes [Gibb et al., 2012]. This novel approach to borehole sealing has the

potential to address some of the uncertainties in seal design, such as long-term degradation of seals and effective sealing within the DRZ surrounding the borehole. The current project expands on these works to evaluate the feasibility of constructing a downhole heater capable of reaching the necessary temperatures to achieve partial meting and to evaluate the viability of performing a field-scale test of the proposed system.

RSI-2492-15-003

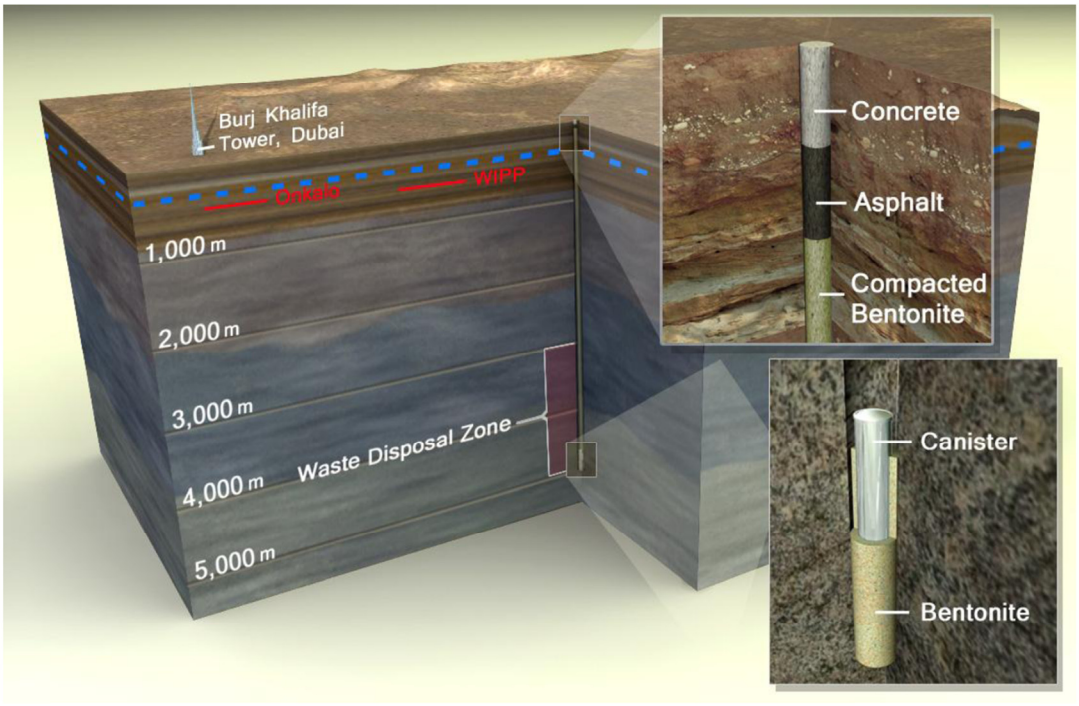

Figure 1-1. Generalized Concept for Deep Borehole Disposal of High-Level Radioactive Waste (From Arnold et al. [2011]).

1.1 RELEVANT DEEP BOREHOLE DISPOSAL RESEARCH

The technical requirements for the effective design of the borehole sealing method for deep borehole disposal of nuclear waste was described by Arnold et al. [2011] and is summarized below:

- Borehole seals must provide a low-permeability barrier to fluid flow within the borehole. The overall permeability of the material used in the seal zone above the waste packages must be less than 1×10^{-12} m^2 [Herrick et al., 2011].
- Borehole seals must form a low-permeability bond with the borehole walls to prevent fluid flow around the seals. The seal material should decrease the permeability of the host rock near the borehole by penetrating fractures and “healing” the DRZ.

- Borehole seals must be durable, particularly during the peak thermal period when the potential for fluid flow is the greatest.
- Borehole seals must have the strength to resist mechanical loads from overlying materials and the potential of overpressuring from below.
- Borehole materials must be chemically stable at 100°C to 200°C for at least 2,000 years, which is the time it takes for the thermal pulse and driving force for vertical fluid movement to pass.
- Borehole materials should have the ability to be amended with compounds that would serve as "getters" to retard the transport of nonabsorbing radionuclides, such as iodine-129 (^{129}I).
- Multiple seals must be used to provide redundant defense in depth, thus maintaining performance even after an individual seal fails.

The feasibility of several sealing materials (including cement and bentonite) are currently being explored. Although traditional sealing materials will provide a low-permeable barrier, the integrity of these materials over a period of thousands of years is uncertain. Another significant limitation of traditional borehole sealing methods is that the ability of these materials to reduce the permeability of the DRZ is also uncertain. The rock melt sealing system proposed by Attrill and Gibb [2003a] has the potential to address the limitations of the traditional borehole sealing methods. The creation of a continuous, recrystallized melt that encompasses the backfill (by way of fine-grained, crushed host rock backfilled into the borehole) and the DRZ essentially creates a seal of material analogous to the host rock. Concerns of enhanced permeability in the DRZ and seal degradation are resolved with the recrystallized rock seal.

Research by Attrill and Gibb [2003a] has included melting experiments carried out under high-pressure conditions (approximately 150 MPa). Their work has revealed melting relationships for granite under water-saturated and -undersaturated conditions. The melting experiments suggest that melting begins just under 700°C and that the amount of melt increases with increasing water content until the vapor saturation is reached at approximately 5 percent. With no added water, only 5 percent of the melt is achieved at a temperature of 850°C, but the addition of 1 percent water generates 40 percent melt at a temperature of 800°C. The data suggest that the benefit of lower melting temperatures with increased water content may diminish as saturation is reached, and once vapor saturation is reached, the amount of melting becomes independent of water content. Furthermore, and just as importantly, the percentage of melt does not increase with increased test duration. Two grain sizes were evaluated to represent backfill materials (less than 90 micrometers [μm] and less than 500 μm); both contained the same phase assemblages and the compositions of the quenched liquids were indistinguishable. Attrill and Gibb also conducted a similar experiment on a core of solid rock. The experiment resulted in the same phase assemblages as the crushed-rock tests, but with less percentage of melt. The melting was initiated at the outer surface of the core and resulted in a distinguishable envelope of glass that permeated through the entire rock core. The

combined results suggest that water saturation has a much greater influence on the percentage of melt than does the grain size of the crushed samples or the test duration of the melting experiment. These tests performed at high pressures are not representative of the current borehole sealing concept where the pressure would be closer to 30 MPa (the weight of the column of drilling fluid at a depth of approximately 3 km). Nevertheless, Arnold et al. [2013] indicate that the change in pressure (30 MPa as opposed to 150 MPa) will likely only raise the solidus by a few dozen degrees Celsius.

A full-scale field test is necessary to evaluate the ultimate feasibility of the deep borehole concept. To that end, a Request for Information (RFI) was released by the Department of Energy (DOE) in the fall of 2014 regarding a deep borehole field test. The primary goals of the deep borehole field test listed in the RFI include the following:

- Test the feasibility of characterizing and engineering deep boreholes
- Test processes and operations for safe emplacement in deep boreholes
- Confirm geologic controls in a deep environment
- Test safety and practicality of the deep borehole disposal and retrieval, as well as borehole sealing concepts.

The RFI solicited the interest of local communities and stakeholders who were willing to host a field test that fulfills the technical and logistical requirements detailed by Arnold et al. [2013]. After the DOE is able to review the responses to the RFI submitted in late 2014, a Request for Proposals may be released in the near future for a full-scale field test of the deep borehole concept. The sample of recent research projects summarized above demonstrates the interest in the deep borehole concept as a repository option and, specifically, the potential for a rock melt sealing system as a means of eliminating some of the uncertainties with traditional sealing concepts.

1.2 PURPOSE AND OBJECTIVES OF THE CURRENT STUDY

The overarching objective of the current study is to evaluate the feasibility of constructing a downhole heater that is capable of meeting the technical and logistical requirements to melt rock. This ultimate objective was accomplished by two primary approaches. The first approach is to define the heater requirements and conceptually design a system that is capable of melting rock. The second approach is to determine the feasibility of conducting an in situ, field-scale melting experiment, which will be necessary to validate the suitability of the rock melt seal. These two approaches are addressed separately below and throughout the report.

Several requirements must be defined for the successful conceptual design of a rock melt sealing system. The primary questions regarding heater design that this feasibility study has attempted to answer include the following:

- What are the power and time requirements for a downhole rock melt heater? Several authors [Attrill and Gibb, 2003a; Arnold et al., 2013] have referenced a power of 12 kilowatt (kW) for their modeling efforts. Is this power requirement still adequate when some of the other material variables are changed?
- What is a reasonable range of thermal properties and melting points that could be encountered in a deep borehole, and how might these properties affect the heater requirements?
- Are "off-the-shelf" products (i.e., resistive-heating elements) available that can be used to provide the preferred power output and withstand the expected downhole conditions (e.g., sustained, high temperatures)?
- How might a conceptual heater be delivered downhole and supplied with power?

Once a conceptual heater design for a rock melt borehole sealing system has been determined feasible, validating the design in a field-scale experiment is imperative. Field-scale tests are required to assess the overall feasibility of the entire deep borehole concept (as indicated by the recent RFI for a deep borehole field test recently released by the DOE) and are especially important for evaluating a new sealing system. Field tests on the rock melt sealing system will be required to confirm that the perceived benefits of the rock melt system can be accomplished and to investigate for potential unforeseen problems.

An ideal test location would be where field conditions are comparable to that of a deep borehole environment (e.g., stress conditions and rock weathering) while allowing access to the test location to evaluate the posttest recrystallized melt. The proposed field area for demonstrating and validating the seal design is located at the former Homestake gold mine in western South Dakota. This large extensive underground infrastructure has been converted into an underground laboratory, which is now referred to as the Sanford Underground Research Facility (SURF) and whose operations are currently funded by the DOE.

The proposed field project would identify appropriate mine levels such that one or more drill holes could be bored from one level to one or two underlying levels (mine levels are generally on 150-foot intervals). Drilling of this nature has been performed recently in the facility, and the engineering staff is well positioned to help with determining the cost and planning for this type of project. This borehole(s) would be used for performing an in situ melting experiment by using the designed electrical heating system. Packer tests would be used to evaluate the effectiveness of the seals. Careful siting of these tests would then allow performing a mine back. This mine back would investigate the degree of melting, the interface between the melt and the country rock, the mechanical stability of the plug, and the hydrologic properties of the plug, as well as any effect on fractures in the country rock if they are present. The information obtained from the mine back will provide an important validation of the effectiveness of the rock melt technology. The primary questions regarding the feasibility of a field-scale test that this study has attempted to answer include the following:

- Is there an adequate location within SURF that could be used for in situ experiments?
- Will the existing infrastructure at SURF support the requirements of an in situ heating experiment, and if not, what types of infrastructure improvements are necessary?
- What are the preliminary costs associated with the proposed experiments?

The completion of the major objectives of this study provide validation of the feasibility of the proposed rock melt sealing concept and a path forward for the future development of a prototype heater and testing of the system.

1.3 REPORT ORGANIZATION

This report contains five chapters including this introduction. The approach, as mentioned above, was divided into two primary sections: feasibility of a heater design and feasibility of a field-scale test location. Chapter 2.0 describes the factors relevant to the heater design. Issues discussed include the impact that variations in (1) thermal properties, (2) melting temperatures, and (3) latent heat will have on the design requirements of the heater components. Numerical modeling results are presented and used to support the conceptual design of the heater components. Chapter 3.0 addresses the feasibility of performing an in situ melting experiment to validate the performance of a rock melt seal, including selecting a site location and characterizing the local rock, describing the melting experiments, and providing a preliminary cost analyses. Chapter 4.0 provides a summary of the overall feasibility of the study and relevant conclusions looking forward. Cited references are listed in Chapter 5.0, followed by the appendices. Appendix A provides supporting information on the numerical modeling efforts and Appendix B documents the laboratory testing and melting experiments performed to determine the thermal properties and melting temperature of the country rock at SURF.

2.0 CONCEPTUAL HEATER DESIGN

A critical stage in the heater design is defining the requirements for the system. The conceptual design is based on the use of an electric, resistive-heating element. The resistive element will emit heat as an electric current is passed through the element according to Joules Law. The amount of heat released is a function of the current, the resistive characteristics of the heating element, and time. The heat generated by the heating element will gradually increase the temperature as a function of distance away from the borehole. The temperature distribution within the backfill and host rock will vary with time and will define the melting front based on the power supplied to the heater, the thermal properties of the surrounding materials, and how long the heater is on.

The target disposal interval for deep borehole disposal is the crystalline rock that occurs at depths between 3 km and 5 km. Wedepohl [1995] classifies the continental crust at these depths as consisting typically of granitic and granodioritic plutons along with metamorphic rocks exhumed from deeper in the crust. For the purpose of the design of the conceptual heater, a range of thermal properties of likely host rock relied on literature research; particularly, previous research conducted by Attrill and Gibb [2003a], Gibb et al. [2008b], and Robertson [1988]. The range of likely thermal properties of the host rock will be used to define the interaction between the three primary design requirements of the heater: power, maximum temperature, and time.

Attrill and Gibb [2003a; 2003b] showed that granite can be partially melted and recrystallized under attainable conditions and on a practical time scale. Their results revealed that partial melting of granite will require temperatures between 700°C and 800°C and, upon cooling, the partial melt will be completely recrystallized at a temperature of approximately 550°C. The melting tests performed by Attrill and Gibb provide the basis for the minimum melting temperature that must be achieved by the heater design.

The goal of the rock melt sealing system is to extend the partial melting front through the DRZ, in effect “healing” the DRZ. Recent studies [Tsang et al., 2004; Shen et al., 2009] suggest the radial extent of the damaged zone induced by a tunnel boring machine extends into the rock between 0.01 m and 0.35 m. This extent is approximately 10 percent or less of the excavation diameter. Drilling-induced damage will likely result in a similar DRZ; however, the extent of the DRZ in a borehole at 3 km may be greater, particularly if anisotropic conditions exist. These estimates are the requirements for the distance that the partial melt must extend into the host rock to seal the DRZ.

2.1 CONCEPTUAL HEATER REQUIREMENTS

The feasibility of the conceptual design depends upon the ability of an electric resistive heater to partially melt the backfill and host rock within a reasonable set of constraints (i.e., temperature, time, and power). Variations in the melting temperature and thermal properties encountered in rocks that could be encountered in a deep borehole may result in significant errors in the calculated power requirements for the conceptual design of an in situ heating system. Previous numerical modeling studies [Arnold et al., 2013; Beswick et al., 2014] have indicated that a 12 kW heater is sufficient to melt granite. Therefore, initial scoping studies were performed assuming a 12 kW heater with a heated length of 1 m to determine the impact that variations in thermal properties have on the heater requirements. Evaluating the impact of different thermal properties focused on the maximum temperatures predicted in the backfill and the temperature distribution versus time in the surrounding host rock. The results of the scoping studies in their entirety are provided in Appendix A. For brevity, the results presented in the body of this report are limited to the summary of the major findings.

The results of the scoping studies suggest that for most of the thermal rock properties anticipated to be encountered in the deep borehole disposal concept, a 12 kW heater will achieve borehole wall temperatures greater than 800°C at 8 days. These results are consistent with numerical modeling performed by Beswick et al. [2014], which revealed a heater 2 m long with a diameter of 0.264 m and a power density of 110 kilowatts per cubic meter (kW/m^3) (i.e., a power output of approximately 12 kW) should be sufficient to obtain partial melt of the backfill and borehole wall.

Figure 2-1 shows the temperature distributions predicted assuming a 12 kW heater and thermal properties of typical granite (thermal conductivity = 2.51 Watts per meter Kelvin [W/m-K], specific heat = 879 Joules per kilogram Kelvin [J/kg-K], and latent heat = 300,000 Joules per kilogram [J/kg] [Gibb et al., 2008b]) at 8 and 32 days. The partial melting front can be delineated by evaluating the predicted temperature distribution with time in conjunction with the experimental data on melting temperatures obtained by Attrill and Gibb [2003a]. Assuming a partial melting temperature of 800°C, the melting front has reached the borehole wall at 8 days, but considerably more time is required to advance partial melting temperatures farther into the host rock. At 32 days, temperatures greater than 800°C extend approximately 15 centimeters (cm) radially from the borehole wall and 17 cm vertically from the base of the heater. Varying the thermal properties from that of typical granite had mixed results and the following significant conclusions can be made from the scoping study:

- Borehole wall temperatures capable of producing a partial melt are achievable under most expected thermal conductivities with a 12 kW heater. However, rock with unusually high thermal conductivity (e.g., pure quartz) is able to transport the heat away from the borehole before melting temperatures can be achieved, regardless of time.

- Porosity of the backfill should not impact the ability to achieve partial melting temperatures in the host rock, but the porosity of the backfill may influence the operation of the heater because temperatures greater than 2,000°C may exceed the temperature rating of conventional heater components.
- Latent heat values had a minimal impact on the temperature distribution around the borehole. Borehole wall temperatures exceeding 800°C were predicted shortly after 36 hours for latent heat values of 271,000 J/kg, 300,000 J/kg, and 419,000 J/kg.

RSI-2492-15-004

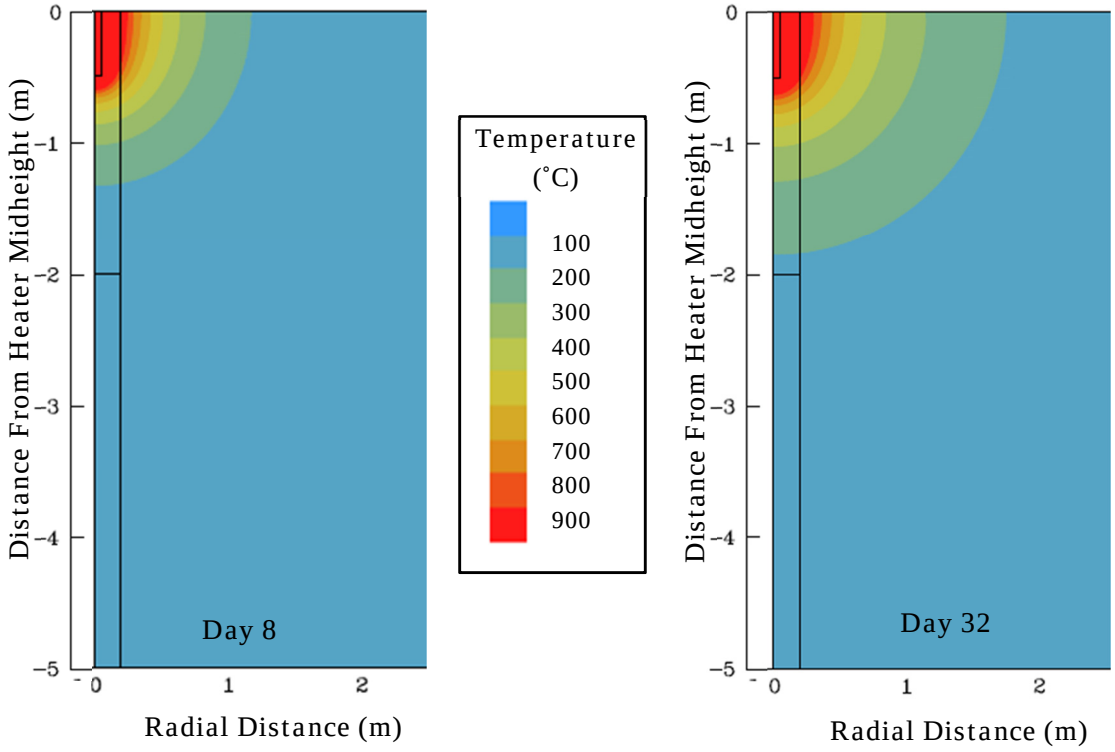

Figure 2-1. Temperature Contours Predicted Surrounding the Borehole Assuming a 12 kW Heater at 8 and 32 Days.

2.2 CONCEPTUAL HEATER DESIGN

Based on the scoping study and previous efforts by others, three variables provided the minimum design constraints for the conceptual heater: power, temperature, and time (respectively, 12 kW, an 800°C partial melting temperature, and at least 8 days that the heater must remain on for the partial melt to reach the borehole wall). The conceptual heater design was divided into three different components: the heating element, the power delivery system, and the heater housing. During the design process, attempts were made to use "off-the-shelf" parts rather than designing new components. In theory, this approach should make the conceptual design significantly less expensive, but it may restrict the limits of some of the design variables; whereas, "custom-build" components could be tailored to the specific

requirements. One such limitation is the sensitivity of the heater components to temperature; consideration must be given to placing components far enough from the heater element that they will remain within their allowable operating temperature ranges. The design requirements, restrictions, and specifications of each heater component are described in the following sections.

2.2.1 Heating Elements

The primary function of the resistive-heating elements is to increase the resistance within the electric circuit, thereby converting electrical energy into thermal energy capable of achieving partial melts of the host rock. Heat transfer simulations of the deep borehole disposal concept indicate that a 12 kW heater is able to achieve borehole wall temperatures greater than 800°C. The results also suggest that the heater must maintain these temperatures for several days to achieve partial melts sufficient to heal the DRZ. Furthermore, the scoping studies have revealed that maintaining a constant 12 kW supply to the heater will result in component temperatures exceeding 2,000°C.

Researching currently available resistive-heating elements resulted in two candidate "off-the-shelf" resistive elements: the I^2R Moly-D and I^2R Starbar heating elements. Both heating elements are capable of providing 12 kW of sustained power and achieving temperatures greater than 1,500°C. The Moly-D element is a dense cement material that consists of molybdenum disilicide and has a high power rating (22.6 Watts per square centimeter [W/cm^2]) at 1,450°C. The Starbar is a resistive-heating element that is made of a special high-density, reaction-bonded silicon carbide that has a maximum watt loading of 11 W/cm^2. The Starbar has the benefit of retaining its rigidity at high temperatures, unlike the Moly-D that begins to soften and bow at temperatures above 1,200°C. However, the Moly-D is capable of operating at temperatures of 1,775°C in an oxidizing atmosphere, as compared to the Starbar that must be operated in an inert atmosphere above 1,370°C. The Moly-D is a low-voltage, high-current element in contrast to the Starbar that is a high-voltage, low-current element. For a maximum power setting of 17 kW, the Starbar will require approximately 220 volts and 80 amps as compared to the Moly-D element that will require approximately 35 volts and 535 amps for the same power setting.

2.2.2 Power Delivery System

The power delivery system is required to provide at least 12 kW and possibly as high as 17 kW of power to the heating element in a corrosive environment at distances greater than 3 km. The Starbar heating element will require between 180 and 220 volts and between 60 and 80 amps. Beswick et al. [2014] point out that similar or greater levels of power are supplied to submersible vehicles by means of an umbilical cord, which operate at greater depths and pressures than those anticipated in the deep borehole disposal concept. The power delivery system must also withstand the tensile force of suspending the heater and resistance from cable lengths exceeding 3 km.

The conceptual power delivery system consists of electromechanical cables containing four power conductors for primary and auxiliary power supply to the heating elements. To support heater voltage (220V) and amperage (80A) requirements, the power cable would require a minimum diameter of 3.8 cm, which would include two size 0000 conductors, thermocouples, mechanical supporting sheath and necessary insulation. The supporting sheath is comprised of special alloy wires with tensile strength of 1,860 MPa to 2,275 MPa. The electrical power is delivered from a surface control station to the heater with variable control alternating current (AC) power supply. It is also envisioned that the power cables will include a breakpoint so that once the power cable is tensioned, the adaptor will break free from the remaining heater components. This feature will allow the power cable to be retrieved even if the heater canister is entombed within the partial melt.

2.2.3 Heater Canister Materials

The primary function of the heater canister is to protect the heating element in the setting and temperatures anticipated in the deep borehole environment. Therefore, the canister must be designed to withstand downhole pressures at depths of 3 km (approaching 35 MPa) and operating temperatures akin to the maximum operating temperature of the heating element. The heater canister must also transfer the energy from the heating element to the canister wall and surrounding backfill. Because the principal mode of heat transfer inside the canister will be thermal radiation, the thermal properties of the canister material also deserve consideration; specifically, the emissivity value of the material. Emissivity is a measure of the effectiveness of a material to emit or absorb thermal radiation; a material that has a greater emissivity value will be more efficient at absorbing the thermal radiation emitted by the heating elements. A single material is likely preferred for constructing much of the canister because differential thermal expansion of dissimilar materials may damage the structural integrity of the unit.

Given these design criteria, commercially available refractory metals have been reviewed, and the materials that meet the minimum melting temperature requirement are provided in Table 2-1. Several potential container materials have a high-emissivity value, including molybdenum, graphite, and possibly stainless steel (if the maximum temperature is further restricted). The expense of some of the more specialized materials can be substantial and, therefore, lower cost options may be preferred. Although several metals meet the design requirements, molybdenum was chosen for the conceptual design because of its high melting point, high emissivity value, and high yield strength.

High yield strength of the canister material is important to the design because it will control the required canister wall thickness to prevent crushing under downhole pressures. Two equations are commonly used to calculate the collapse pressure of casings [Timoshenko, 1976]. Equation 2-1 assumes a perfectly round casing, and Equation 2-2 accounts for eccentricity in the casing. The collapse pressures are defined by:

$$P_{cr} = \frac{2E}{\left(1-\nu^2\right)\left(\frac{D}{t}-1\right)^3} \tag{2-1}$$

where:

P_{cr} = perfect-cylinder collapse pressure (MPa)

E = Young's modulus for molybdenum (MPa)

ν = Poisson's ratio for molybdenum (–)

D = outside diameter of canister (m)

t = wall thickness of canister (m).

$$P_d^2 - \left\{\frac{2Y_p}{\frac{D}{t}-1} + \left[1+3\left(\frac{D}{t}-1\right)e\right]P_{cr}\right\}P_d + \frac{2Y_p P_{cr}}{\left(\frac{D}{t}-1\right)} = 0 \tag{2-2}$$

where:

P_d = design collapse (MPa)

Y_p = material yield strength (MPa)

e = eccentricity constant (≈ 0.01).

Table 2-1. List of Potential Heater Canister Material and Material Properties Pertinent to the Conceptual Heater Design

Metal	Density (kg/m^3)	Melting Point (°C)	Thermal Conductivity (W/m-K)	Emissivity (–)	Yield Strength[(a)] (MPa)
Stainless Steel	7,850	1,510	35	0.87	240
Titanium	4,510	1,670	20	0.51–0.61	100
Platinum	21,500	1,770	73	0.07–0.11	125
Chromium	7,150	1,860	90	0.27–0.66	140
Molybdenum	10,200	2,620	140	0.80–0.84	415
Tantalum	16,400	2,980	54	0.19–0.31	90
Tungsten	19,300	3,400	168	0.15–0.28	344
Graphite	2,230	3,642	160	0.78–0.85	4,137

(a) Reported values are the minimum strengths values.

Assuming a Young's modulus of 3.30×10^5 MPa, a Poisson's ratio of 0.307, and a yield strength of 415 MPa for molybdenum, an outside diameter of 30.5 cm, and a wall thickness of 4.5 cm, the calculated collapse pressure for a perfectly round casing is approximately 3,630 MPa; however, accounting for eccentricity in the casing results in a collapse pressure of approximately 120 MPa, which is equivalent to a factor of safety of 3.4. The minimum wall thickness required to prevent the canister from crushing under a downhole pressure of 35 MPa is 1.5 cm.

The heater canister design is further subdivided into three sections: (1) the "hot" section that contains the heating element, (2) the insulated "cold" section that contains the heating power housing, and (3) a sinker bar to overcome buoyancy and allow the heater to drop to the preferred depth. It is envisioned that the hot and cold sections will need to be completely sealed (likely welded) to prevent drilling fluid from contacting the heating element and other critical components. The connection with the sinker bar is less crucial and can likely be fastened by screws.

2.2.3.1 Hot Section

The heating elements will be contained in the hot section that consists of a 1-m-long by 30.5-cm outside diameter (OD) pure molybdenum tube with a wall thickness of 4.5 cm, as shown in Figure 2-2. The 30.5-cm OD allows for an average of 6.25 cm of annular space surrounding the container in the anticipated 0.43-m-diameter borehole. The bottom of the housing (referenced to downhole) is closed and flat. The housing will accept one primary and at least one auxiliary heating element. A single heating element is capable of providing the power and temperature requirements; additional elements are included for redundancy of the system. The heating elements are supported and fastened by ceramic bushing support centralizer collars located at the heating element terminal cold end. The heater container has been represented as an idealized cylindrical canister that does not include any extended surfaces (i.e., fins) to increase the heat transfer rate to the surrounding backfill. Extended surfaces could be used to increase the heat transfer rate to the backfill and decrease the temperatures predicted in the heater and will be further evaluated in future designs. Thermocouple wells are located adjacent to the heating element hot zone and, if feasible, at the downhole end as well. The uphole housing end is designed with a sleeve receptacle for the heating element power housing (cold section).

2.2.3.2 Cold Section

The cold section consists of a 1-m-long by 30.5-cm OD molybdenum tube with a wall thickness of 4.5 cm, as shown in Figure 2-3. The primary function of the cold section is to provide adequate distance from the resistive-heating elements to isolate temperature-sensitive components. Therefore, the power housing unit is designed with a ceramic partition to insulate the interior of the cold section from the heating element; temperatures within the borehole are expected to vary across the cold section from a high of approximately 1,000°C nearest the hot

section to a low of 300°C at the uphole end. Bus bar connectors within the power housing unit are designed to accept uphole electromechanical cable conductors and downhole braided conductors that are fastened to the heating element terminal ends. Thermocouple wells are also located at the bus bar/heating element terminal and the bus bar/electromechanical terminals. The housing is open and sleeved on the downhole end to assemble to the heating element housing. The housing is open on the uphole end and contains a sleeve receptacle to accommodate an adaptor. The adaptor consists of 0.25-m by 30.5-cm OD tube with a wall thickness of 4.5 cm. The adaptor is sleeved on the downhole end to join with the power housing and transitions on the uphole end to accept the sinker bar and logging cable.

RSI-2492-15-005

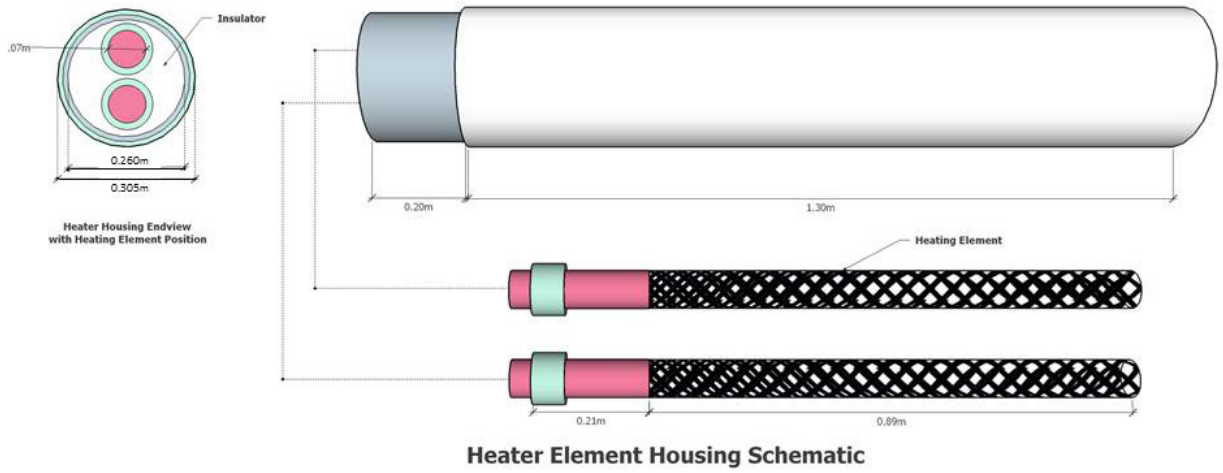

Figure 2-2. Schematic Illustrating the Conceptual Heater Power Housing Hot Section.

RSI-2492-15-006

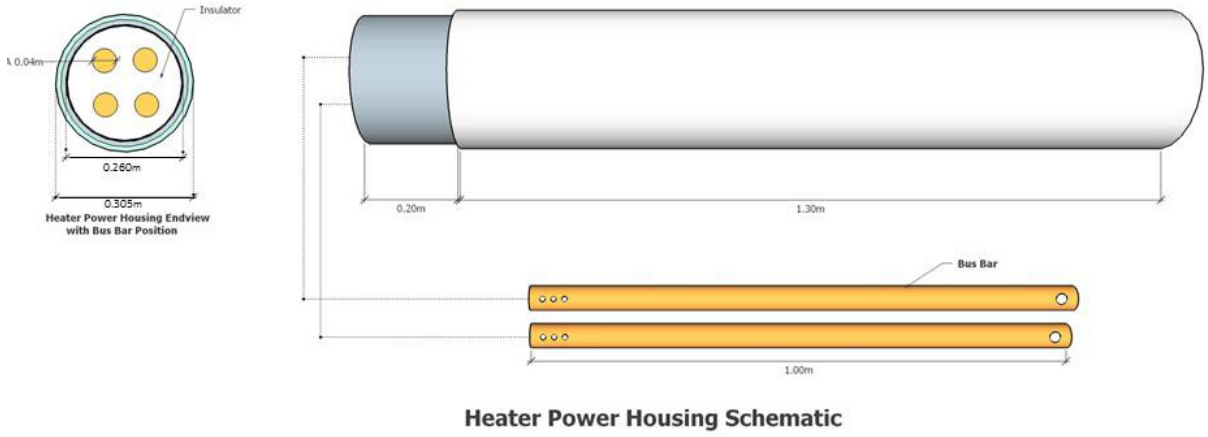

Figure 2-3. Schematic Illustrating the Conceptual Heater Power Housing Cold Section.

2.2.3.3 Sinker Bar

The main objective of the sinker bar is to increase the weight of the heater and allow gravitational force to overcome buoyancy within the fluid-filled borehole so that the heater can descend to the preferred depth. When the heater enters the well fluid, fluid pressure will exert a force essentially equally in all directions across the heater. However, because there is effectively less surface area at the top of the heater than at the bottom of the tool because of the electomechanical cables connections, a greater force is exerted against the bottom of the tool, which pushes the tool up if not counteracted by the weight of the heater and sinker bar. Preliminary calculations for the power delivery system suggest that the minimum cable diameter required is 1.5 cm. At a depth of 3 km, an additional 3,500 kg will be required to counteract the unbalanced force acting on the heater assembly. The results of the scoping studies suggest that the base of the sinker bar will be exposed to temperatures as high as 300°C, which requires that the sinkbar material to have a melting temperature that exceeds this requirement. The final length of the “cold” section may need to be extended to provide adequate separation from excessive temperatures if the melting temperature of the material is less than 300°C.

3.0 DESIGN OF AN IN SITU MELT EXPERIMENT

Several authors [Brady et al., 2009; Arnold et al., 2011 and 2013] have recommended that the in situ testing of seal designs is necessary to evaluate their effectiveness, and this would especially be the case for a new and innovative system such as the rock melt borehole seal. The objective of the proposed in situ melt experiment is to address several key questions that relate to the functionality and integrity of the rock melt concept for sealing the borehole for the deep borehole disposal; specifically:

- What degree of confidence can be placed in achieving a melt plug seal?
- Is the DRZ effectively eliminated through the melting and recrystallization process?
- How effective is the bond between the melt plug and the country rock?

The in situ melt experiment proposed herein will attempt to address each of these questions through several in situ melting experiments using the conceptual heater design. It is envisioned that to validate the in situ melt concept, access to the boreholes in which the in situ melting experiments are performed will be required. Access to the melt will allow the degree of melting, the interface between the melt and the country rock, the mechanical stability of the plug, and the hydrological properties of the plug to be evaluated.

3.1 PROPOSED EXPERIMENT LOCATION

The former Homestake gold mine in western South Dakota provides an ideal location to perform an in situ melting experiment. The mine, which had been operated for over 125 years, was converted into an underground laboratory in support of science and engineering research. The laboratory, referred to as the Sanford Underground Research Facility (SURF), is owned by the state of South Dakota and funded by the DOE in support of high-energy particle physics experiments. The underground area donated to South Dakota by Barrick Gold Corporation consists of 7,700 acres surrounding the facility, and the surface facility footprint consists of 186 acres [Heise, 2014]. The surface infrastructure at SURF is well established and the sole purpose of the facility is to support the science operations. The surface infrastructure, shown in Figure 3-1, includes an administration building, a science and education center, surface laboratories, core storage, water treatment plant, and the two headframe complexes: the Yates Shaft and the Ross Shaft. These two shafts provide ingress/egress to the underground workings and the main laboratories located on the 4850 Level.

Heise [2014] described the current state of the physics experiments that are being conducted at SURF in the laboratories on the 4850 Level. The experiments currently ongoing include searches for dark matter by the LUX (Large Underground Xenon) collaboration and the Majorana Demonstrator (MJD) project. The objective of the MJD project is to determine

whether or not neutrinos are their own antiparticles and to determine properties of neutrinos, such as mass. Other areas of the underground facility are being prepared for the CASPAR project, which is a facility to characterize stellar reactions. In addition to these experimental laboratories, preinstallation geotechnical drilling and assessments are being conducted in support of the Long Baseline Neutrino Experiment (LBNE). The SURF site, known as the Long Base Neutrino Facility (LBNF) would act as a detector for a neutrino beam generated at the Fermi National Laboratory at Batavia, Illinois.

RSI-2492-15-007

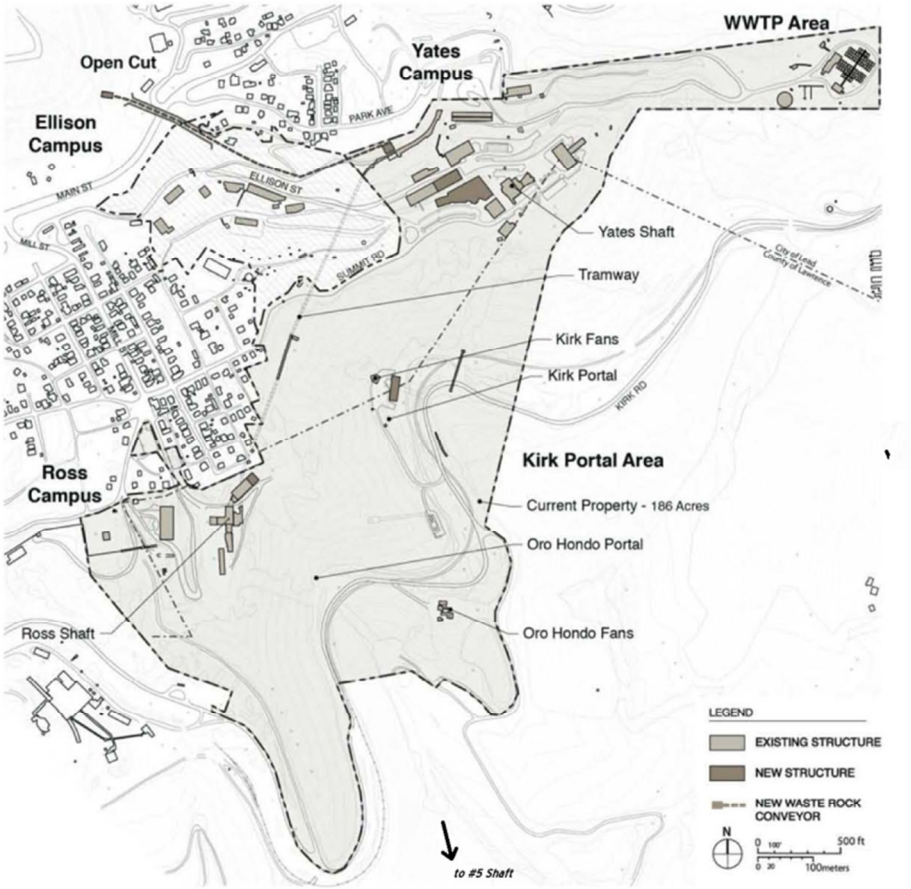

Figure 3-1. Surface Facilities Supporting the Operations of the Sanford Underground Research Facility.

3.2 IDENTIFICATION OF POSSIBLE TEST SITES

All of the current physics experiments are located on the 4850 Level, but a wealth of other drifts, shafts, and raises are available throughout the underground facility. Figure 3-2 shows a long section of the underground workings wherein the levels are projected into the line of section. The levels of the mine were typically developed at 45.75-m (150-foot [ft]) intervals below the 1100 Level. Only a small fraction of the old workings are currently maintained. Some

unmaintained areas could be put into service; whereas, other areas located within the ore body (Homestake) that were primarily mined for ore extraction are not available. The region in the vicinity of the Ross Shaft Station on the 1700 Level appears to be a good candidate for the purposes of this feasibility evaluation. This location has the advantage of being in an area that does not impinge on other experiments or potential operations of the underground infrastructure, and it also has the advantage that any additional infrastructure, such as requirements for added electrical runs, is closer to the surface and the Ross Shaft, so costs are reduced.

RSI-2492-15-008

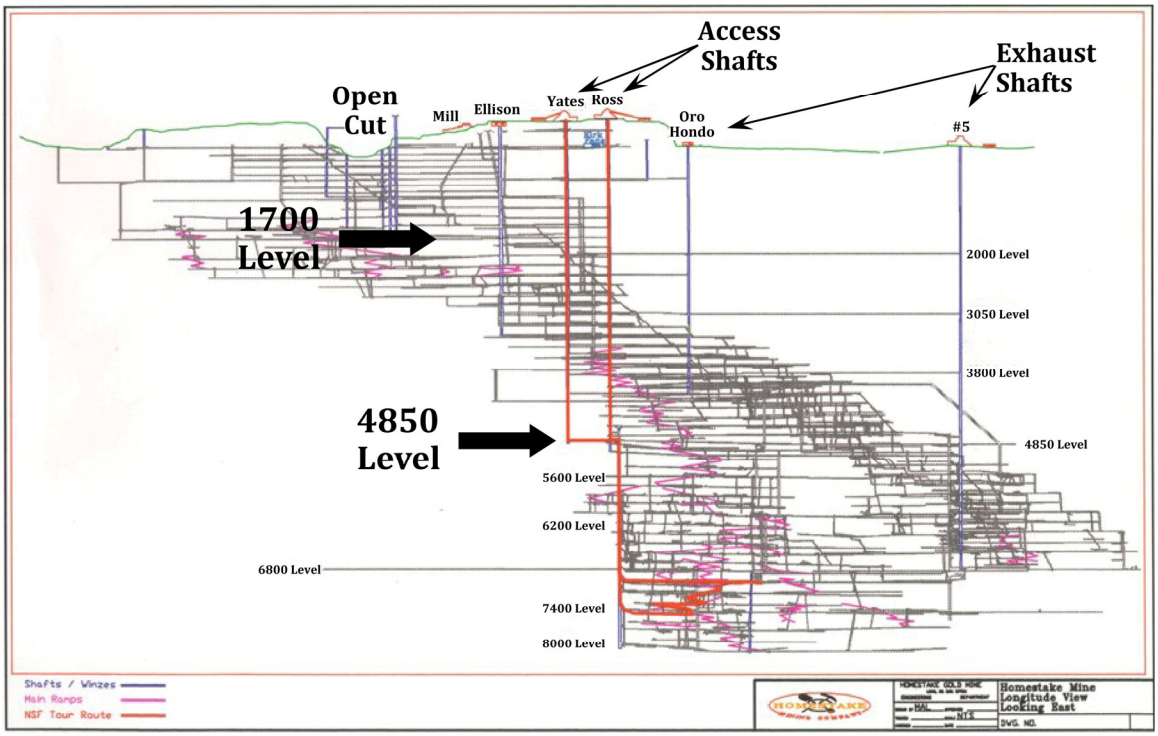

Figure 3-2. Long Section of the Underground Workings at the Sanford Underground Research Facility.

Figure 3-3 shows a portion of the 1700, 1850, and 2000 Level drifts in the vicinity of the Ross Shaft Station superimposed upon each other. At this location, the three mine levels are well aligned above each other, which allows access to the rock package at levels extending more than 90 m vertically. This alignment provides an excellent opportunity to drill from the upper level (1700 Level) to the lower level (2000 Level) with access to the melt from the intermediate level (1850 Level), which fulfills one of the design requirements for a mine-back investigation of the melt.

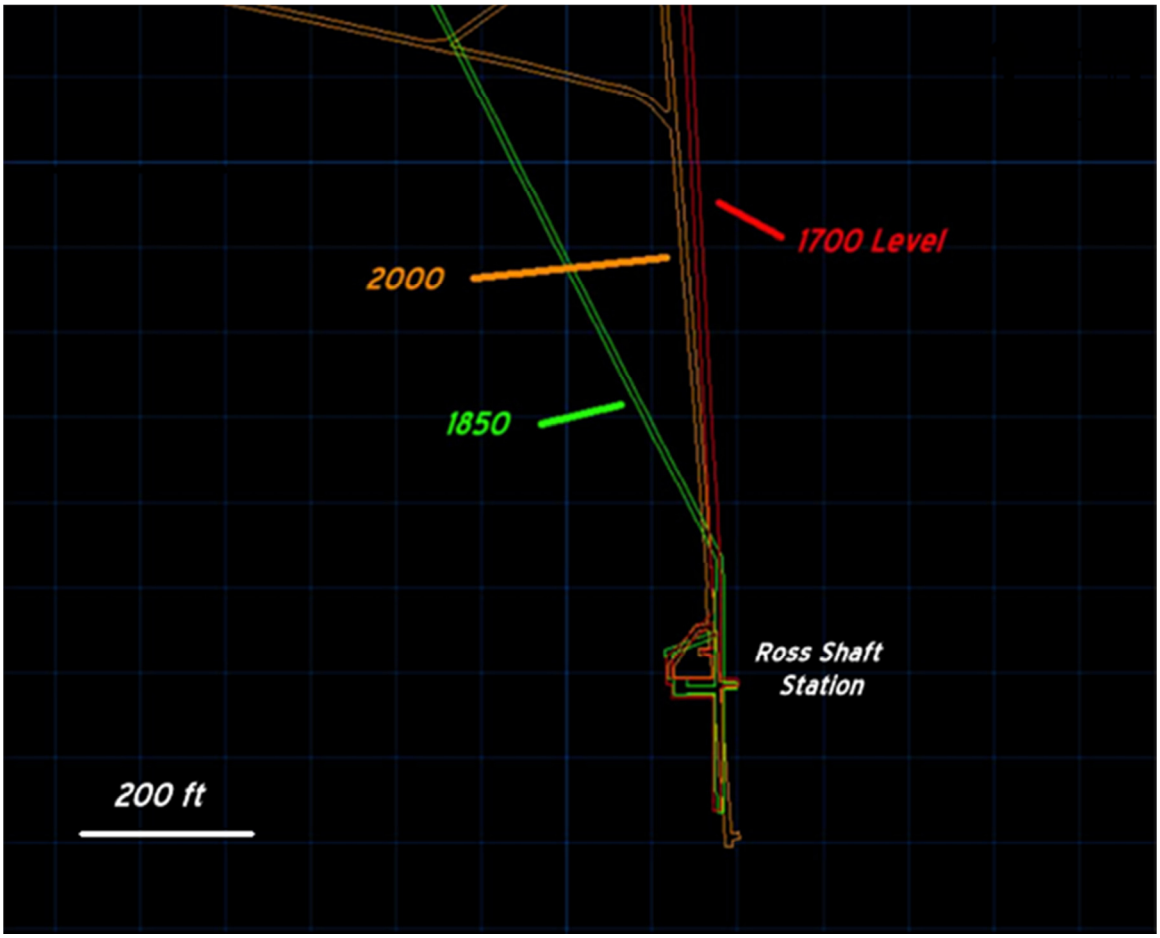

Figure 3-3. The Drift Infrastructure for the 1700, 1800, and 2000 Levels Near the Ross Shaft Station.

3.3 REQUIRED CHANGES AND IMPROVEMENTS TO THE CURRENT SANFORD UNDERGROUND RESEARCH FACILITY INFRASTRUCTURE

The 1700, 1850, and 2000 Levels near the Ross Shaft Station were examined to determine their current condition with regard to the infrastructure and ground support and identify concerns relevant to the field-scale melting experiment. The following sections describe the findings.

3.3.1 1700 Level

The general condition of the 1700 Level is favorable for the proposed field testing. A direct connection exists between the Ross Shaft and the Yates Shaft, so secondary egress is well established. The track linking those shafts is in good condition. Recent drilling from the 1700 Level to the 2000 Level was conducted that resulted in a 1.04-m (41-inch) borehole that is

now part of the water-control system. This hole ensures that water will not interfere with operations on the Ross Shaft side, which is favorable for the proposed project. In general, ground conditions are good and only minor rock bolting would be required for occupying a drilling site.

A cutout will be required to allow sufficient room for the drill to pull rods, which would be minor excavation work. A similar expansion of the drift was necessary for the previous drilling on this level and it was easily accomplished.

3.3.2 1850 Level

The 1850 Level is not regularly maintained and is only accessible on the Ross Shaft side for the first 56.4 m of the drift away from the shaft, although it is possible to access other parts of the 1850 Level via a ramp system between the 1700 and 2000 Levels. The drift is plugged at a point 56.4 m (185 ft) from the Ross Shaft with an engineered concrete dam to control water flow in other parts of the underground. Examination of the 1850 Level near the Ross Shaft Station shows that the rock is in very good condition. It has no rock bolts throughout its history, and the current condition does not appear to require any additional ground support, although a conservative estimate would probably include minor rock bolting as a precaution. The shaft station is in good shape and no work is anticipated to be required. However, when heavy equipment is delivered at a station, a common practice is to set the cage “down on chairs.” Chairs are two supports that extend from the cage to firmly support the cage at a station. The 1850 Level does not have a place for the chairs to land so a minor amount of work will be required to install those supports.

The condition of the plug on the 1850 Level is good with no signs of bulging or cracking. Therefore, safe access is assured on the 1850 Level that would support potential mine-back operations to examine the melted plug.

3.3.3 2000 Level

The 2000 Level is one of the main levels maintained in the facility and is important for water control and ventilation. Therefore, the level is well maintained with good track, ground control, and ventilation. This level was one of the earliest experiment locations during the first phases of the laboratory, and some experiments still have instrumentation in areas distant from the Ross Shaft Station. No substantive work on the infrastructure on this level would be required. Safe access for mine-back excavations could also be performed on the 2000 Level.

3.4 CHARACTERIZATION OF THE TEST LOCATION

The Sanford Underground Research Facility is located in the northern Black Hills in Lead, South Dakota, in a sequence of Proterozoic metamorphic rocks (shown in Figure 3-4) that were

intruded by rhyolites during the Tertiary approximately 55 million years ago. A significant amount of data currently exists on the geology at SURF. Four formations are predominantly exposed underground at SURF: (1) the Poorman Formation, (2) the Homestake Formation, (3) the Ellison Formation, and (4) the Yates Formation. The oldest rock is the Yates Formation, which was originally a basaltic unit. The overlying metasedimentary formations were primarily clastic sedimentary rocks with the exception of the Homestake Formation, which is an iron formation.

RSI-2492-15-010

Figure 3-4. Stratigraphic Section of the Geological Units Encountered Near the Sanford Underground Research Facility.

Although originally a sedimentary sequence of shale, siltstone, and sandstone, metamorphism, including folding and shearing have altered the rock and Figure 3-5 illustrates a generalized structure of the geology [Caddy et al., 1991]. In general, the rocks form a large-scale structure that plunges steeply to the south. A shell of intensely folded metasedimentary rocks (the Poorman and Ellison Formations) surround a broader fold in the mafic core of the structure represented by the metabasalt (amphibolite) of the Yates Formation. This sequence of approximately 2-billion-year-old rocks was intruded by rhyolite dikes at approximately 55 million years ago based upon radiometric dating of nearby intrusions [Duke, 2005]. The rhyolite intrusions are generally aphanitic, although some phases of the rhyolites contain phenocrysts of quartz and extend from the surface to the deepest mapped portions of the underground workings. Although individual bodies of rhyolite may not be continuous from one level to another, the bodies are sufficiently abundant such that they constitute a significant percentage of the rock within the zone. Rhyolite is the fine-grained equivalent of the granitic rocks likely to be encountered at a deep borehole disposal site and is the target unit for in situ melting tests.

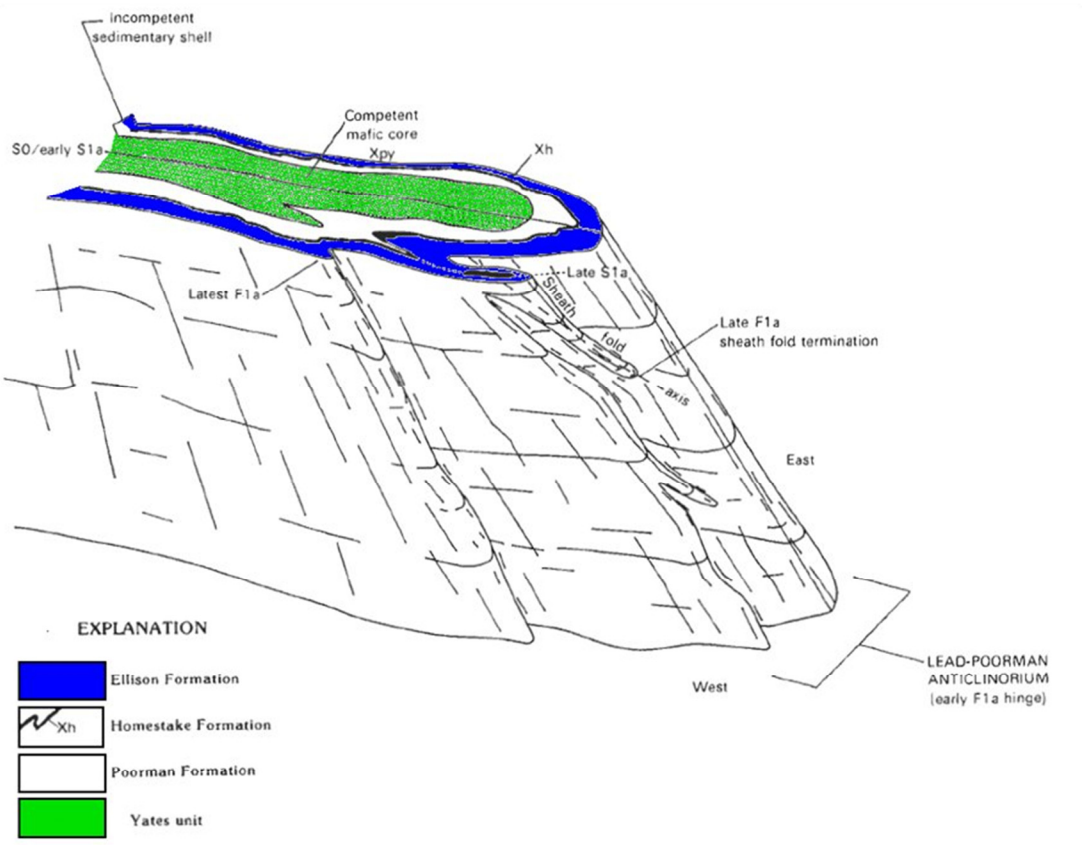

Figure 3-5. Generalized Structure of the Geological Units Encountered Near the Sanford Underground Research Facility.

The geology near the Ross Shaft Station is well known because of careful mapping of the drifts and extensive drilling during the mine life. This mapping has been compiled into a database used by the Vulcan mine design system, which is available for planning experiments. Figure 3-6 shows a portion of the 1700 Level near the Ross Shaft. The rhyolite dike (yellow contour) has intruded into the Ellison Formation (blue contour), the Homestake Formation (brown contour), and the Poorman Formation (white contour). The geology on this level has been characterized by drift mapping, core drilling, and extrapolation of units above and below this level. Although mapping individual rhyolite bodies is not possible using the available information, the zone of intrusions is clearly well defined and dips steeply to the east. The yellow rhyolites are squared on their southern extremities because of the lack of geological control but undoubtedly continue to some distance.

3.4.1 Melting Temperatures

Attrill and Gibb [2003a] have previously performed melting experiments to determine partial melting of typical S-type (sedimentary protolith) crustal granites. However, these experiments were carried out under pressures greater than 0.15 GPa and water concentrations between

0 percent and 5 percent weight. Water content is known to significantly reduce the melting temperatures of rock and, depending upon the experimental methods, may not be present at the proposed SURF test site. Therefore, additional melting experiments were carried out at the South Dakota School of Mines & Technology to determine the melting temperatures of rhyolite under dry conditions. The melting experiments are described in detail in Appendix B, and the results are summarized in the following text.

RSI-2492-15-012

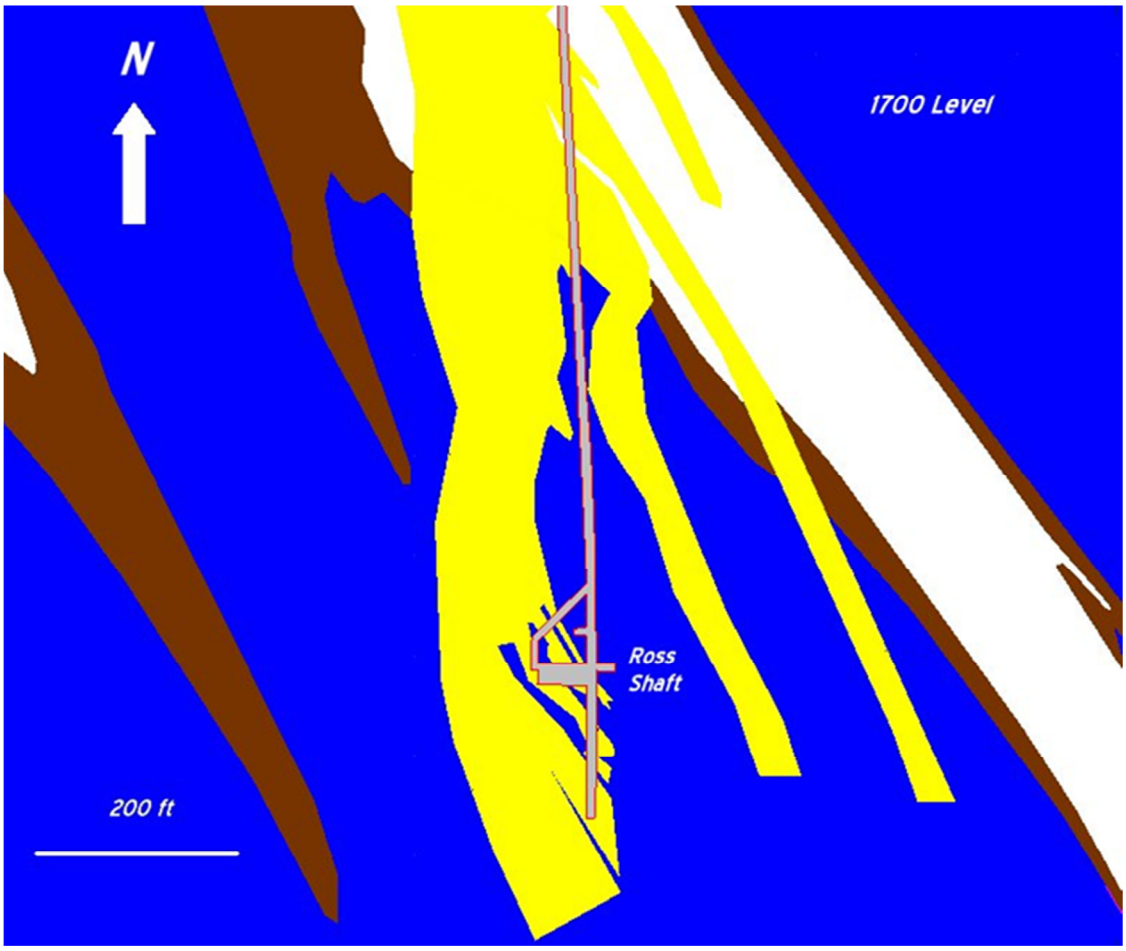

Figure 3-6. Geology on the 1700 Level Near the Ross Shaft.

To determine the approximate temperature of the liquidus, melting experiments were carried out between 1,100°C and 1,700°C on crushed samples of rhyolite. At the conclusion of the 1,100°C melting experiment, the rhyolite sample was still unconsolidated; therefore, it was determined that no melt had been generated. By contrast, the melting experiment performed at 1,700°C resulted in an amalgamated mass. Subsequent melting experiments were performed at 50°C intervals to define the partial melting temperature of the rhyolite. The results of these experiments revealed that the partial melting temperature of the rhyolite begins between 1,400°C and 1,450°C and the liquidus occurs below 1,500°C.

3.4.2 Thermal Properties

Thermal property tests were performed to determine the thermal conductivity (k) and specific heat (c_p) values for both intact and crushed rhyolite as well as for the intact Ellison Formation. The temperature dependence of each property was determined by conducting tests at temperatures between 20°C and 262°C. Table 3-1 lists the average thermal conductivity and specific heat values determined for the rhyolite and Ellison samples, and the values are plotted in Figures 3-7 and 3-8. The specific heat values listed in Table 3-1 were calculated by dividing the laboratory-derived volumetric heat capacity by the density of the specimen: 2,588 kg/m^3 and 3,034 kg/m^3 for rhyolite and Ellison, respectively. In general, the results of the tests are consistent with the anticipated behavior of most rocks—the thermal conductivity decreases with increasing temperature, while specific heat increases as the temperature increases.

Table 3-1. Thermal Conductivity, Specific Heat, and Volumetric Heat Capacity of Rhyolite and Ellison

Temperature (°C)	Rhyolite			Ellison		
	Thermal Conductivity (W/m-K)	Specific Heat (J/kg-K)	Volumetric Heat Capacity (J/m^3-K)	Thermal Conductivity (W/m-K)	Specific Heat (J/kg-K)	Volumetric Heat Capacity (J/m^3-K)
20	2.54	666.31	1,724,085	1.58	203.15	616,422
38	2.42	742.54	1,921,340	1.57	223.62	678,531
66	2.35	822.54	2,128,333	1.55	248.17	753,028
94	2.37	829.1	2,145,327	1.50	266.92	809,912
122	2.37	852.03	2,204,657	1.46	275.99	837,439
150	2.31	874.19	2,261,980	1.41	285.78	867,152
178	2.26	888.98	2,300,265	1.37	296.92	900,970
206	2.20	897.16	2,321,436	1.33	298.92	907,013
234	2.18	913.58	2,363,907	1.30	305.79	927,871
262	2.13	935.59	2,420,863	1.27	311.84	946,221

The thermal conductivity values obtained from the crushed, dry rhyolite are significantly less than those determined for the intact rock. The conductivity is similar between the different porosity values tested, but slightly greater thermal conductivity was measured for lower porosity values. Although the thermal conductivity values for the crushed rhyolite were significantly less than those of the intact rhyolite, these values are consistent with thermal conductivity values of dried sand, which typically ranges between 0.15 W/m-K to 0.25 W/m-K.

RSI-2492-15-013

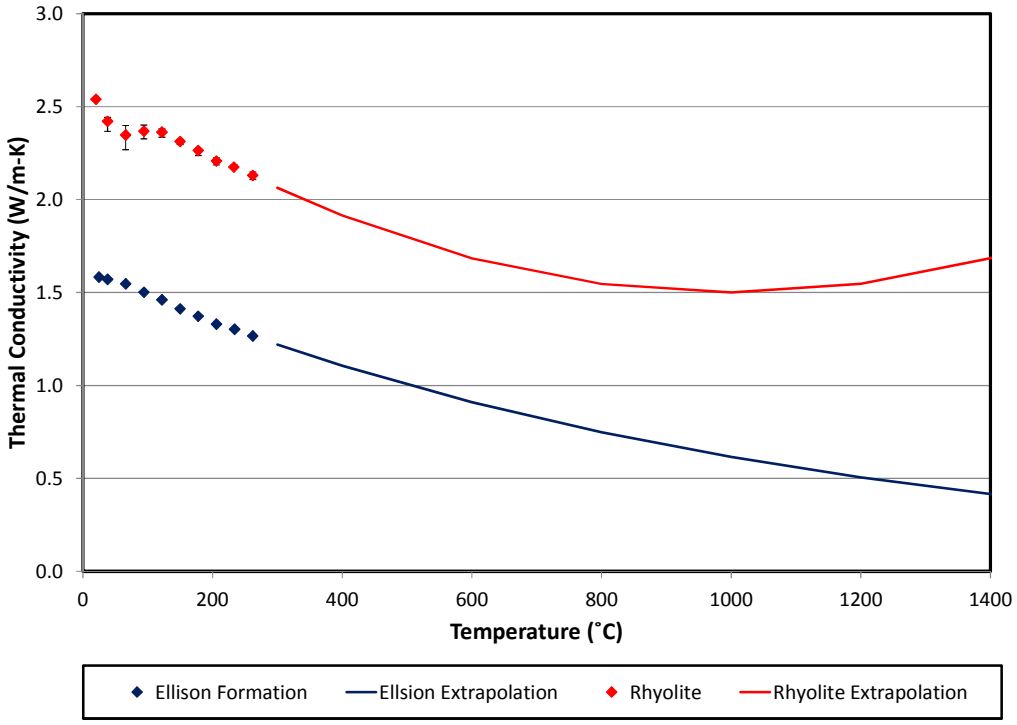

Figure 3-7. Measured and Extrapolated Thermal Conductivity Values for Rhyolite and Ellison Samples.

RSI-2492-15-014

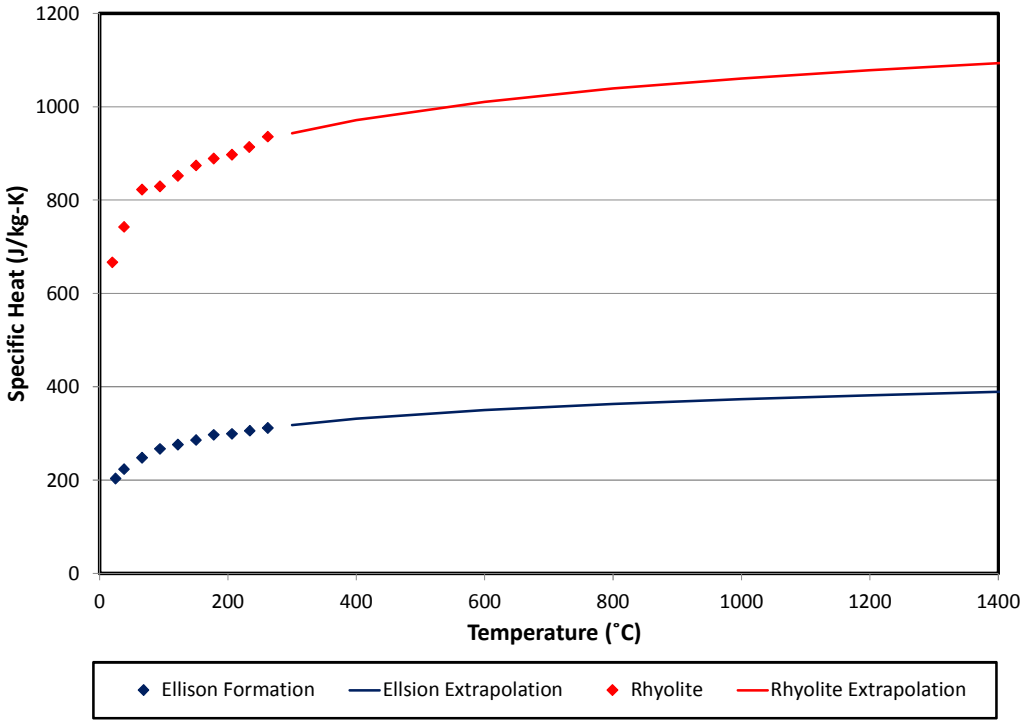

Figure 3-8. Measured and Extrapolated Specific Heat Values for Rhyolite and Ellison Samples.

The maximum temperature settings on the laboratory heater limited the characterization of the thermal properties to temperatures below 300°C. Therefore, the thermal conductivity and specific values were extrapolated based on data available for the temperature dependence of thermal conductivity and specific heat of similar rocks [Robertson, 1988]. The measured laboratory results and extrapolated values are also plotted in Figures 3-7 and 3-8. The extrapolated values of thermal conductivity continue to decrease with increasing temperatures; however, at temperatures greater than 1,000°C, the thermal conductivity values for the rhyolite begin to increase. This behavior is the result of the influence of the quartz content in the rhyolite, which causes the thermal conductivity to increase at temperatures greater than 700°C.

3.5 SANFORD UNDERGROUND RESEARCH FACILITY HEATER REQUIREMENTS

The results of the scoping studies suggest that the conceptual heater design is capable of attaining temperatures of a partial melt (1,400°C and 1,450°C) determined for dry rhyolite. However, the significantly greater melting temperatures in the absence of water required additional numerical studies to estimate the power and time required to melt the backfill and country rock. Additional simulations were performed by using the melting temperature (1,400°C) and thermal properties (k = 2.50 W/m-K, c_p = 1,100 J/kg-K) determined from laboratory testing on intact, dry rhyolite specimens. The highest measured thermal conductivity from the laboratory tests was used because it is more conservative, even though the actual thermal conductivity will likely be lower at the higher temperatures. Because the latent heat of the rhyolite is still uncertain, a conservative value of 300,000 J/kg was assumed. Thermal conductivity and specific heat values of 0.50 W/m-K and 400 J/kg-K, respectively, were assumed for the backfill material based on the laboratory results for crushed rhyolite. However, after melting has been predicted in the backfill, the thermal properties revert back to those of the intact rhyolite. The conceptual heater design was centered within a 0.2-m-diameter borehole and provided a constant power of 12 kW. The heater was encapsulated within a backfill material that extends 1.5 m above and below the heater, and the ambient temperature at SURF was conservatively assumed to be 20°C.

The results of these simulations focused on the heat transfer to the surrounding country rock and the required power to achieve a successful partial melt of the backfill and borehole wall located within a rhyolite dike. The conservative assumptions made for the thermal properties and partial melting temperature are designed to produce a robust heating system that is capable of exceeding the requirements of a deep borehole environment.

Figure 3-9 presents the heater canister temperature, borehole wall temperature, and the temperature 5 cm into the rock as a function of time. The temperature of the heater (red curve) increases rapidly but becomes nearly constant after a short period of time. The temperature of the borehole wall (blue curve) exhibits a similar trend, exceeding 1,400°C after 5 days. However, even after 30 days, the temperature 5 cm into the rock (green curve) is only 1,350°C.

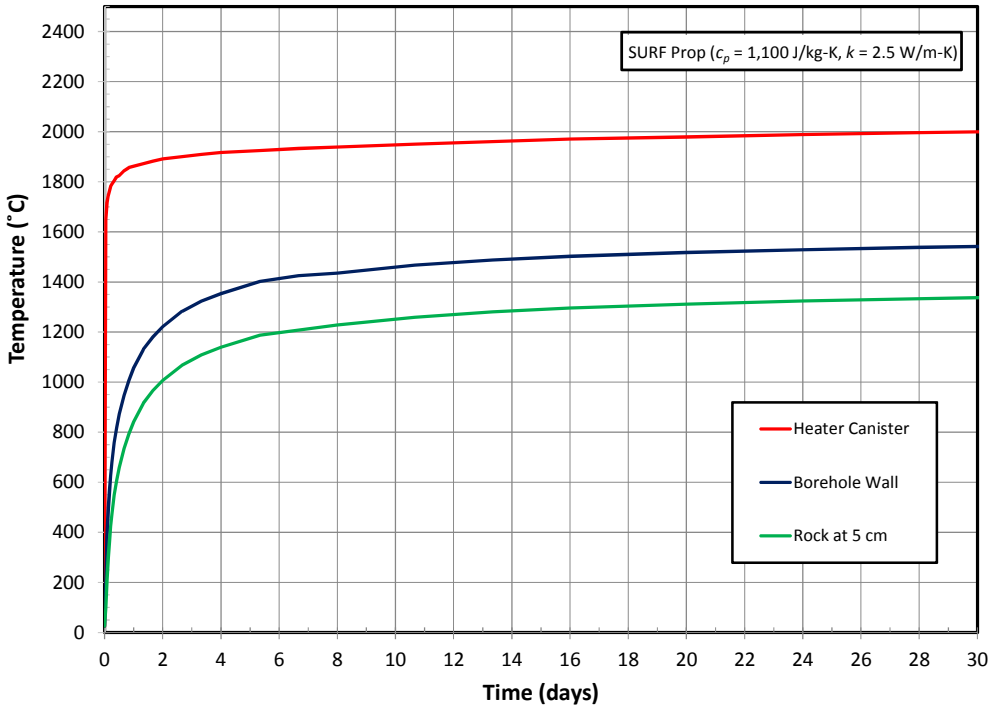

Figure 3-9. Predicted Temperature Versus Time for Different Locations on the Midheight of the Sanford Underground Research Facility Heater.

Figure 3-10 shows the predicted rock temperature at 2 days, 8 days, and 32 days as a function of radial distance from the midheight of the heater. At 2 days (blue curve), the entire backfill has achieved temperatures greater than 1,400°C. The borehole wall exceeds 1,400°C at 8 days; however, temperatures greater than 1,400°C are only predicted 3 cm into the country rock after 32 days. Figure 3-10 also shows that temperatures greater than 800°C extend approximately 15 cm radially from the borehole wall at 32 days.

Figure 3-11 displays temperatures for the same times along the vertical distance of the borehole axis. Comparison of the curves reveals the rock temperature rapidly decreases away from the heater, and the temperatures predicted at 3 m in the host rock are nearly ambient (20˚C). Temperatures greater than 800°C extend approximately 17 cm axially from the base of the heater at 32 days. These results suggest that at a distance of as little as 3 m away, the experiments will raise the rock temperature only a few degrees. A target experiment location can be placed fairly near an existing drift with heat loss to the drift being minimal, which will allow a relatively short distance to complete a mine back and access the posttest recrystallized melt.

RSI-2492-15-016

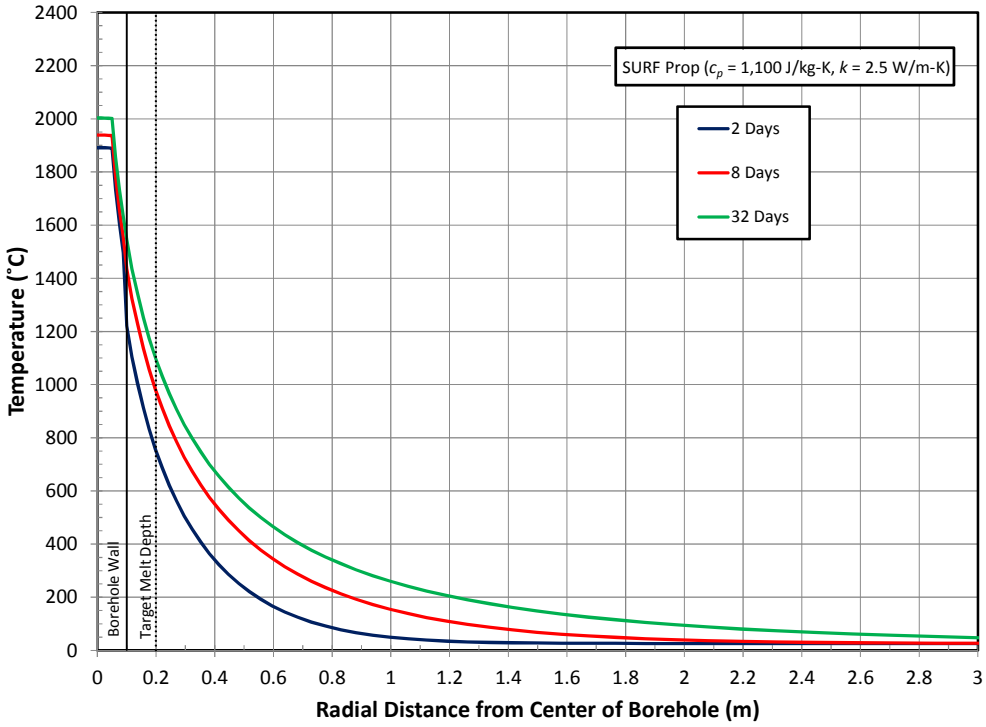

Figure 3-10. Predicted Temperature Versus Radial Distance at the Midheight of the Sanford Underground Research Facility Heater.

RSI-2492-15-017

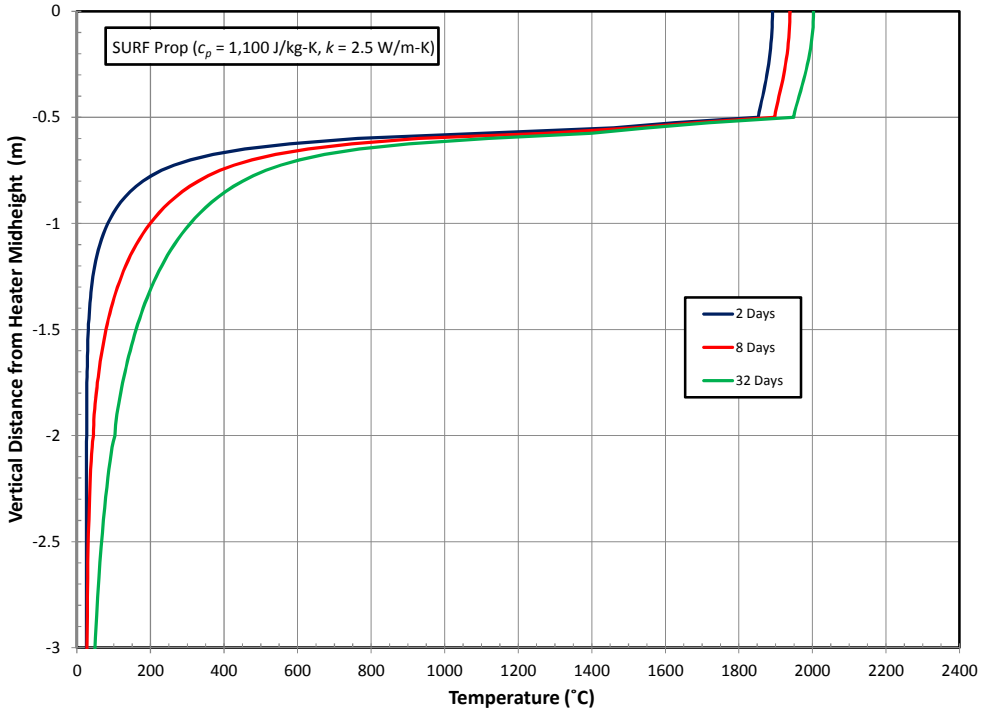

Figure 3-11. Predicted Temperature Versus Axial Distance From the Midheight of the Sanford Underground Research Facility Heater.

These results suggest that even under conservative conditions (specifically, a 1,400°C melting point of dry rhyolite), the backfill may be melted after 2 days and that a partial melt of the borehole wall may be achieved after 8 days; however, extrapolating the data suggests a partial melt 10 cm into the rock may require approximately 2 years for a 12 kW heater. Although the time required to achieve a partial melt through the entire DRZ may be unrealistic under these constraints, successfully completing melting tests in this environment will provide confidence that the system is easily capable of producing an effective seal under more favorable conditions.

3.6 COST ANALYSIS

A suitable test location has been identified at the SURF and site inspections performed on the 1700, 1850, and 2000 Levels have revealed the proposed experimental locations are in good conditions. The technical and logistical requirements for performing the field-scale melting experiments can be met by using or expanding the existing infrastructure at SURF. Major factors that influence the cost of the field-scale melting experiment include remediation and maintenance requirements; drilling expenses, including the number and size of boreholes; and electrical power and time required to perform the melting experiments. Heat transfer simulations have revealed backfill melts may be achieved within 5 days, but it may take greater than 30 days to achieve partial melts around the boreholes.

Table 3-2 itemizes a preliminary estimate of the major expenses associated with the field-scale melting experiment. Although these costs are preliminary, the estimates are based on comparable projects from drillers, SURF staff, and outside vendors experienced with working at the SURF site. The costs provided in Table 3-2 are divided according to costs associated with preexperimental site preparation costs, experimental costs, and a 25 percent contingency. Major preexperimental costs include developing an alcove to house the experiment off of the main drift, minor rehabilitation and rock bolting to protect the ingress and regress routes, drilling the boreholes for the heater tests, and electrical costs associated with extending the current infrastructure to the test site. Six test holes are considered for the preliminary estimate. An overview of the experiment work includes characterizing the borehole geology, determining the baseline in situ hydraulic conductivity through the DRZ, heater construction and borehole instrumentation costs, melting costs, postmelt in situ hydraulic conductivity test, and mine-back expenses to assess the integrity of the melt. The preliminary estimate for the field-scale testing of the heater design is approximately $500,000. This preliminary experiment cost includes several conservative estimates and can likely be reduced as estimates are refined. Nevertheless, the preliminary costing indicates that a field-scale melting experiment is feasible within a Phase II Small Business Innovation Research (SBIR) budget while allowing sufficient budget for refining the heater design, coordinating the test program, and interpreting the results. More details on the proposed field test including objectives, procedures, instrumentation, and overall budget will be included in the Phase II Application.

Table 3-2. Preliminary Cost Estimates for a Field-Scale Melting Experiment at the Sanford Underground Research Facility

Activity	Unit	Unit Rate ($)	Number of Units	Total Costs ($)
Preexperimental Costs				
Site Preparation Expenses				
Alcove Mining	number of blasts	3,000	5	15,000
Installing Chairs	lump sum	8,500	1	8,500
Ground Support and Ventilation	included in contingency	0	0	0
Drilling Expenses				
Mobilization/Demobilization	trip	12,000	1	12,000
Drilling Rate, Including Setup, Moving, and Drilling	day	3,650	40	146,000
Equipment (e.g., drill bits, back reamer)	lump sum	15,000	1	15,000
Drilling Consumables	included in contingency	0	0	0
Power Supply Expenses				
15 kVA Transformer	each	2,700	1	2,700
300kVA Skid Mount Transformer, 12kV/480V	each	40,000	1	40,000
12 kV Cable	feet	100	120	12,000
12kV Termination Kits	each	500	2	1,000
Miscellaneous Wire, Hardware, and Fittings	lump sum	2,000	1	2,000
Labor	man hour	51	200	10,200
Preexperimental Total				**$264,400**
Experimental Costs				
Hydraulic Conductivity				
Packer Tests, pre- and postmelt	test	2,000	12	24,000
Borehole Instrumentation	included in contingency	0	0	0
Melting Tests				
Heaters, Components, and Manufacture	each	10,000	6	60,000
Power	lump sum	15,000	1	15,000
Mine Back				
Mine Back to Access Melt	number of blasts	3,000	12	36,000
Experimental Total				**$135,000**
Contingency	percent	25		99,850
Total Experimental Costs				**$499,250**

4.0 SUMMARY AND CONCLUSIONS

The long-term disposal of nuclear waste continues to be an issue of national (and international) importance. The BRC report [2012] states, "...this nation's failure to come to grips with the nuclear waste issue has already proved damaging and costly and it will be more damaging and more costly the longer it continues…." Deep geological disposal is the most promising and widely accepted method currently available for long-term disposal of nuclear waste, and deep borehole disposal, in particular, is an option that has received attention in recent years because numerous factors suggest it is an inherently safe method of disposal [Arnold et al., 2011; 2013]. Some of the uncertainty associated with the long-term suitability of the deep borehole option is related to (1) the degradation of traditional sealing materials over time and (2) the inability of traditional sealing methods to adequately seal the DRZ surrounding the borehole. The rock melt sealing system proposed by Attrill and Gibb [2003a; 2003b] has the potential to alleviate these uncertainties by creating a continuous recrystallized melt that encompasses both backfill materials and the host rock.

This study has evaluated the feasibility of constructing a downhole heater that is capable of meeting the technical and logistical requirements to melt rock. This ultimate objective was accomplished by (1) defining the heater requirements and evaluating a conceptual system capable of melting rock and (2) determining the feasibility of conducting an in situ, field-scale melting experiment necessary to validate the suitability of the rock melt sealing system. The evaluation and conceptual design of the heater system resulted in the following primary findings:

- Borehole wall temperatures capable of producing a partial melt are achievable under most expected thermal conductivities with a 12 kW heater. However, rock with unusually high thermal conductivity (e.g., pure quartz) is able to transport the heat away from the borehole before melting temperatures can be achieved, regardless of time.
- Expected porosity of the backfill should not impact the ability to achieve partial melting temperatures in the host rock, but greater backfill porosities may influence the operation of the heater because temperatures greater than 2,000°C may exceed the temperature rating of conventional heater components.
- Uncertainty in latent heat values have a minimal impact on the temperature distribution around the borehole. Borehole wall temperatures exceeding 800°C were predicted shortly after 36 hours for latent heat values of 271,000 J/kg, 300,000 J/kg, and 419,000 J/kg.
- Commercially available components have been identified that meet the requirements of the heater system, including resistive elements capable of providing the required heat generation, container materials that can withstand the anticipated temperatures, and a system capable of providing power to the heater.

These results suggest that the proposed system is commercially viable and warrant constructing and testing a prototype. Testing the heater in a system analogous to a deep borehole environment is not trivial, but it is necessary to validate the overall suitability of the rock melt sealing system. The Sanford Underground Research Facility (an underground research laboratory) has been identified as a host site for field testing of prototype heaters. The feasibility of performing field-scale experiments in SURF was also evaluated as part of this study and resulted in the following major findings:

- A suitable test location has been identified at SURF. This location will allow in situ testing of the rock melt sealing system in rhyolite dikes (the fine-grained equivalent of granite). In situ hydraulic conductivity test using packers can test the effectiveness of the rock melt seal. Careful drilling and test siting will allow a mine back to be performed from a lower level so that the recrystallized melt can be retrieved and further evaluated in a laboratory.
- The technical and logistical requirements for performing the rock melt tests can be met by using or expanding the existing infrastructure at the SURF with on-site personnel (e.g., blasting) and contractors (e.g., drilling).
- The preliminary cost estimates for the proposed field-scale tests indicate that a field-scale melting experiment is feasible within a Phase II SBIR budget.

In summary, the rock melt sealing concept has the potential to reduce uncertainty associated with a significant issue facing the nation, long-term disposal of nuclear waste. Preliminary efforts defining the requirements of a downhole heater system capable of melting rock indicate that developing a system is feasible using available technology. The next logical step is designing and manufacturing prototype heaters. Concurrent with prototype development is coordinating robust field-scale experiments that are capable of validating the design for potential users.

5.0 REFERENCES

Arnold, B. W., P. V. Brady, S. J. Bauer, C. Herrick, S. Pye, and J. Finger, 2011. *Reference Design and Operation for Deep Borehole Disposal of High-Level Radioactive Waste*, SAND2011-6749, Sandia National Laboratories, Albuquerque, NM.

Arnold, B. W., P. V. Brady, S. Altman P. Vaughn, D. Nielson, J. Lee, F. Gibb, P. Mariner, K. Travis, W. Haldey, J. Beswick, and J. Tillman, 2013. *Deep Borehole Research: Demonstration Site Selection Guidelines Borehole Seals Design, and RD&D Needs*, SAND2013-9490P, Sandia National Laboratories, Albuquerque, NM.

Attrill, P. G. and F. G. F. Gibb, 2003a. "Partial Melting and Recrystallization of Granite and Their Application to Deep Disposal of Radioactive Waste, Part 1 – Rationale and Partial Melting," *Lithos*, 67, pp. 103–117.

Attrill, P. G. and F. G. F. Gibb, 2003b. Partial Melting and Recrystallization of Granite and Their Application to Deep Disposal of Radioactive Waste, Part 2 – Recrystallization," *Lithos*, 67, pp, 119–133.

Beswick J. A., F. G. F. Gibb, and K. P. Travis, 2014. "Deep Borehole Disposal of Nuclear Waste: Engineering Challenges," *Proceedings of the Institution of Civil Engineering*

Blue Ribbon Commission, 2012. "Blue Ribbon Commission on America's Nuclear Future: Report to the Secretary of Energy," *www.state.nv.us*, available online *http://www.state.nv.us/nucwaste/news2012/pdf/brc120126final.pdf*

Brady, P. V., B. X. Arnold, G. A. Freeze, P. N. Swift, S. J. Bauer, J. L. Kanney, R. P. Rechard, and J. S. Stein, 2009. *Deep Borehole Disposal of High-Level Radioactive Waste*, SAND2009-4401, Sandia National Laboratories, Albuquerque, NM.

Caddy, S. W., R. L. Bachman, T. J. Campbell, R. R. Reid, and R. P. Otto, 1991. "The Homestake Gold Mine, an Early Proterozoic Iron-Formation-Hosted Gold Deposit, Lawrence County, South Dakota," Chapter J, *U.S. Geol. Surv. Bull.* 1857, 67 p.

Duke, G. I., 2005. *Geochemistry and Geochronology of Paleocene-Eocene Alkalic Igneous Rocks, Northern Black Hills, South Dakota and Wyoming*, Ph.D. dissertation, South Dakota School of Mines &Technology, Rapid City, SD, 291 p (unpublished).

Gibb, F. G. F, N. A. McTaggart, K. P. Travis, D. Burley, and K. W. Hesketh, 2008a. "High-Density Support Matrices: Key to the Deep Borehole Disposal of Spent Nuclear Fuel," *Journal of Nuclear Materials*, v. 374 (3), pp.370–377.

Gibb, F. G. G., N. A. McTaggart, K. P. Travis, and D. Burley, 2008b. "A Model for Heat Flow in Deep Borehole Disposals of High-Level Nuclear Waste," *J. Geophys. Res.*, vol. 113, Issue B5.

Gibb, F. G. F., K. P. Travis, and K. W. Hesketh, 2012. "Deep Borehole Disposal of Higher Burn Up Spent Nuclear Fuels," *Mineralogical Magazine*, vol. 76(8), pp. 3003–3017.

Herrick, C., B. Arnold, T. Hadgu, R. Finley, P. Vaughn, and P. Brady 2011. *Deep Borehole Seals,* Sandia National Laboratories, Albuquerque, NM.

Heise, J., 2014. "The Sanford Underground Research Facility at Homestake," *arxiv.org* arXiv:1401.0861v1 [physics.ins-det], January 5, 14 p.

McBirney, A. R. 1984. *Igneous Petrology,* Freeman, San Francisco, CA.

Robertson, E. C., 1988. *Thermal Properties of Rocks,* Open-File Report 88-441, prepared by the United States Department of the Interior Geological Survey, Reston, VA.

Robertson, E. C. and D. L. Peck, 1974. "Thermal Conductivity of Vesicular Basalt From Hawaii," *Journal of Geophysical Research*, Vol. 79, pp. 4875–4888.

Timoshenko, S. P., 1976. *Strength of Materials*, 3rd Ed., Krieger Publishing Co., Huntington, NY.

Tsang C.-F, T. Bernier, and C. Davies, 2004. "Geohydromechanical Processes in the Excavation Damaged Zone in Crystalline Rock, Rock Salt, and Indurated and Plastic Clays," *International Journal of Rock Mechanics & Mining Sciences*, 42(1), pp. 109–125.

Shen B., O. Stephansson, M. Rinne, K. Amemiya, R. Yamashi, S. Toguri, and H. Asano. 2009. "FRACOD Modeling of Rock Fracturing and Permeability Change in Excavation-Damaged Zones," *International Journal of Geomechanics*, 11(4), pp. 302–313.

Svalstad, D. K., 1989. *Documentation of SPECTROM-41: A Finite Element Heat Transfer Analysis Program,* DOE/CH/10378-1, prepared by RESPEC, Rapid City, SD, for the U.S. Department of Energy, Chicago Operations Office, Argonne, IL.

Wedepohl, K. H., 1995. "The Composition of the Continental Crust," *Geochimica et Cosmochimica Acta 59,* pp. 1217–1232.

APPENDIX A

HEAT TRANSFER ANALYSIS

APPENDIX A
HEAT TRANSFER ANALYSIS

The material transport property, thermal conductivity (k), and the material thermodynamic property, specific heat (c_p) are required to calculate temperature distributions throughout the rock as a function of time. Thermal conductivity is a measure of the ability of a material to conduct heat and is fundamental in determining the heat loss to the surrounding country rock. A rock with greater thermal conductivity will transport the heat farther from the heater, requiring more energy to reach the melting temperature on the borehole wall. Thermal conductivity is primarily influenced by intermolecular spacing; as such, the thermal conductivity of solids is greater than that of liquids, which is greater than that of a gas. Specific heat is a material thermodynamic property and is defined as the energy required to raise the temperature of a unit mass of a substance by 1 degree. For modeling purposes, specific heat is necessary to calculate the energy required to raise the country rock to the melting temperature. The final factor that must be considered is the latent energy or latent heat of the rock. Latent energy is the energy associated with the binding forces between the molecules of a substance; latent heat of fusion is the amount of energy absorbed during melting. The magnitude of latent heat will depend upon the temperature and pressure at which the phase change occurs.

Because variations in the melting temperature and thermal properties of rocks could result in significant errors in the calculated power requirements for the conceptual heater design, heat transfer analyses were performed to assess the impact that variations in thermal properties would have on the temperature distributions and heater requirements. The two-dimensional, finite element program **SPECTROM-41** [Svalstad, 1989] was used to simulate the heat transfer from the heating element to the surrounding rock. The results of the heat transfer simulations are described in the next section followed by a description of the specialized computer program and finite element models.

A.1 RESULTS OF THE DEEP BOREHOLE SIMULATIONS

Initial scoping studies were performed to determine the impact thermal conductivity, specific heat, backfill porosity, and latent heat has on the temperature versus time distributions predicted around a borehole. The heat transfer simulations represented a 12 kilowatt (kW) heater that is 1-meter (m) long with a 0.1-m diameter centered within a 0.4-m-diameter borehole. The heater was encapsulated within a backfill material that extends 1.5 m above and below the heater. Although circulation of mud during drilling will perturb the ambient temperature distribution in the immediate vicinity of the borehole, these perturbations will have a negligible long-term effect. Consequently, the ambient temperature at the depth of the heater was assumed to be 100°C.

A.1.1 Effects of Thermal Conductivity and Specific Heat on Temperature Distributions

The thermal conductivity and specific heat values of rock are temperature dependent. Data [Robertson, 1988] are available for the temperature dependence of thermal conductivity and specific heat of materials similar to crustal granites; unfortunately, the characterization of the temperature dependence is not known over the full temperature range anticipated in the deep borehole disposal concept. For their studies, Gibb et al. [2008] assumed a thermal conductivity of 2.51 Watts per meter Kelvin (W/m-K) and a specific heat of 879 Joules per kilogram Kelvin (J/kg-K). To determine the impact variations in thermal conductivity and specific heat values may have on the temperature distribution and the power requirements of the conceptual heater design, simulations were performed assuming two additional endpoints of thermal conductivity and specific heat. The values of thermal conductivity used for the scoping study ranged from a low of 1.5 W/m-K (representative of some sandstones) to a high of 8.0 W/m-K (representative of pure quartz). Similarly, for the anticipated temperature and rock compositions, specific heat values of 500 J/kg-K and 1,200 J/kg-K were selected.

The effect that changes in thermal conductivity and heat capacity values have on the temperatures predicted at the heater midheight is illustrated in Figures A-1 and A-2. Figure A-1 presents the rock temperature predicted at 16 days as a function of radial distances from the midheight of the heater for the different thermal properties. A comparison of the curves reveals that thermal conductivity has a significant impact on the predicted temperature distributions and that the rock temperature rapidly decreases away from the heater. At a radial distance of 3 m, the temperatures predicted in the host rock remain at the ambient temperature (100°C), regardless of the thermal properties. At 16 days, a borehole wall temperature of 1,764°C was predicted for thermal conductivity and specific heat values of 1.5 W/m-K and 500 J/kg-K (green curve), respectively. Assuming thermal properties more typical of granite (k = 2.51 W/m-K and c_p = 879 J/kg-K [Gibb et al., 2008]) results in a borehole wall temperature of 1,095°C. Further increasing the thermal conductivity and specific heat to 8.0 W/m-K and 1,200 J/kg-K (red curve), respectively, decreased the borehole wall temperature to 436°C, which is well below the target borehole wall temperature of 800°C.

Figure A-2 presents the borehole wall temperature (radial distance of 0.2 m from the center of the borehole) predicted at the midheight of the heater as a function of time for the thermal properties evaluated. The borehole wall temperatures increase rapidly but become nearly constant after a short period of time. Borehole wall temperatures exceeding 800°C are predicted within 0.5 day for thermal conductivity and specific heat values of 1.5 W/m-K and 500 J/kg-K (green curve) and within 1.25 days for 2.51 W/m-K and 879 J/kg-K (blue curve). However, even after 30 days, the borehole wall temperature predicted for a thermal conductivity and specific heat of 8.0 W/m-K and 1,200 J/kg-K (red curve) is 470°C. Increasing the power of the heater to 15 kW (red dashed curve) only increased the borehole wall temperature at 30 days to 565°C. *These results suggest that borehole wall temperatures capable of producing a partial melt are achievable under most circumstances; however, conditions may arise where the thermal*

RSI-2492-15-018

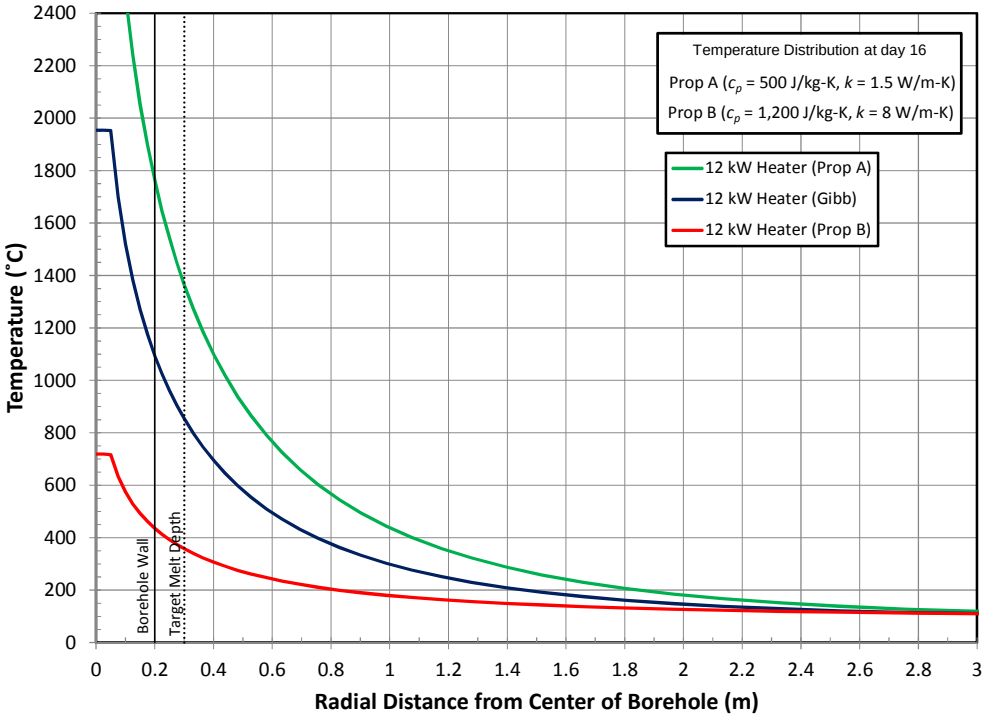

Figure A-1. Temperature Versus Radial Distance Predicted at the Heater Midheight at 16 Days for Different Thermal Properties.

RSI-2492-15-019

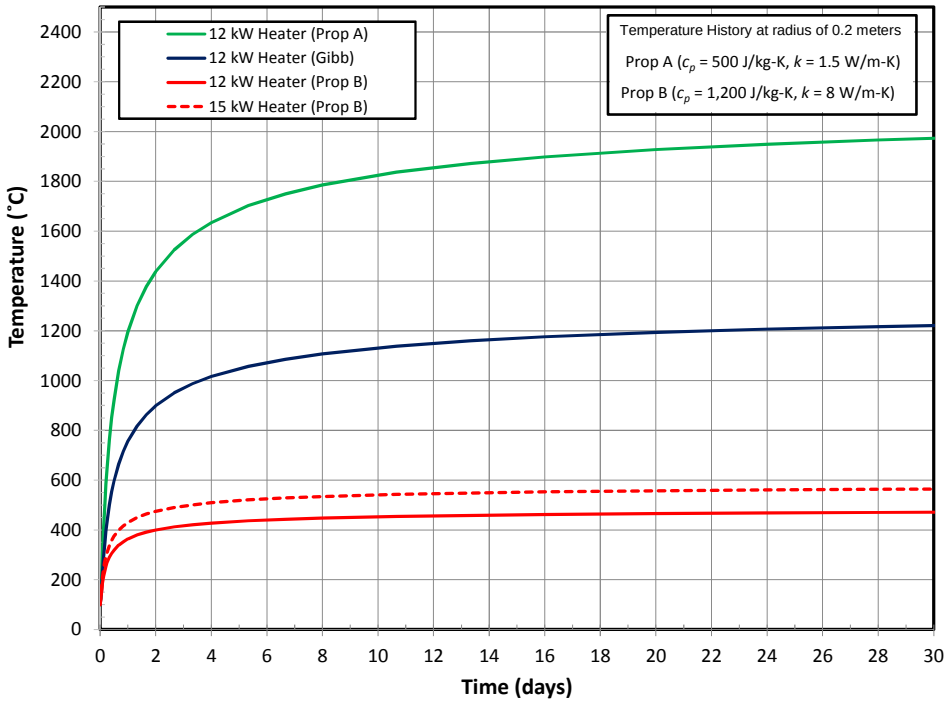

Figure A-2. Borehole Wall Temperature Versus Time Predicted at the Heater Midheight for Different Thermal Properties.

conductivity of the rock transports the heat away from the borehole too quickly and the requirements for an electric resistive heater become unfeasible.

A.1.2 Effects of Backfill Porosity

A reasonable assumption is that the thermal properties of the backfill must be between that of the host rock and those of the fluid present in the borehole. To determine the impact porosity may have on the temperature distribution and the power requirements for the conceptual heater design, a porosity relationship determined by Robertson and Peck [1974] for basalt was used to calculate the thermal properties of the backfill for different porosities. Because of the uncertainty in the composition of the fluid present in the borehole, the borehole fluid was conservatively assumed to have the same properties as water (because drilling fluid would be expected to have a greater conductivity than water). The thermal properties of the backfill were assumed to vary from those of the host rock (k = 2.51 W/m-K and c_p = 879 J/kg-K [Gibb et al., 2008]) based on the relationship defined by Robertson and Peck [1974]. Additional thermal properties calculated for porosities of 10 percent, 25 percent, and 50 percent are provided in Table A-1 along with those of the host rock and water. The thermal conductivity and specific heat values calculated for porosities between 0 percent and 100 percent are similar to thermal conductivity values of moist sand, which typically range between 0.2 W/m-K to 2.0 W/m-K.

Table A-1. Assumed Thermal Properties for Porous Backfill Saturated With Water

Porosity (%)	Thermal Conductivity (W/m-K)	Specific Heat (J/kg-K)	Solidity Squared γ^2
0[(a)]	2.51	879	1.00
0.1	2.18	1,125	0.81
0.25	1.74	1,446	0.56
0.5	1.19	1,851	0.25
1	0.750	2,175	0.00

(a) Properties consistent with Gibb et al. [2008].

The effect of backfill porosity on the predicted temperatures is illustrated in Figures A-3 and A-4. Figure A-3 presents the rock temperature predicted at 16 days as a function of radial distance along the midheight of the heater for different values of backfill porosity. A comparison of the curves in Figure A-3 reveals backfill porosity has a significant effect on the temperature distribution throughout the backfill, with greater temperatures predicted for greater porosity values. However, backfill porosity has only a limited impact on the temperature predicted in the host rock. At 16 days, the borehole wall temperatures varied between 1,094°C and 1,145°C for

RSI-2492-15-020

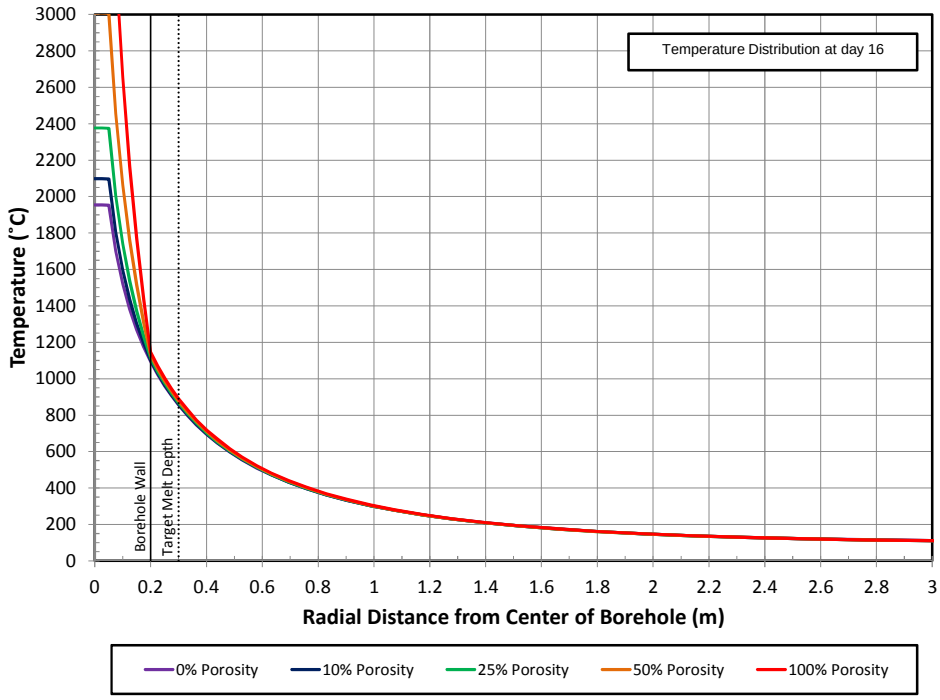

Figure A-3. Temperature Versus Radial Distance Predicted at the Heater Midheight at 16 Days for Different Backfill Porosities.

RSI-2492-15-021

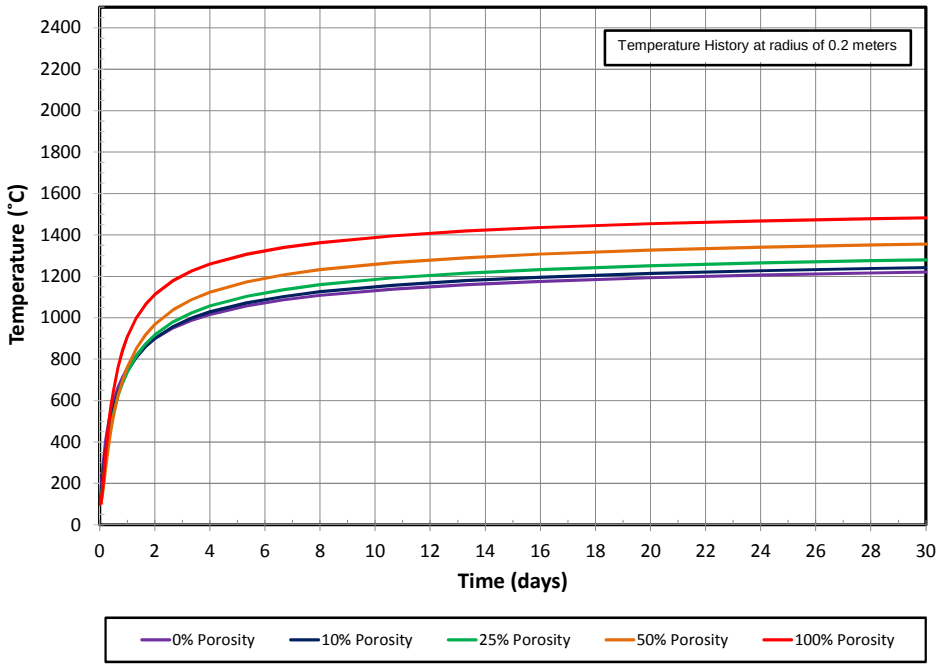

Figure A-4. Borehole Wall Temperature Versus Time Predicted at the Heater Midheight for Different Backfill Porosities.

porosities between 0 percent and 100 percent. Figure A-4 displays the borehole wall temperature (located a radial distance of 0.2 m from the center of the borehole) predicted at the midheight of the heater as a function of time. The temperature response is similar for all backfill porosity values modeled; the borehole wall temperature initially increases rapidly before leveling off. Slightly greater temperatures are predicted for greater backfill porosity values, but borehole wall temperatures greater than 800°C are predicted for all backfill porosity scenarios evaluated. *These results suggest that the porosity of the backfill should not impact the ability to achieve partial melting temperatures in the host rock, but the porosity of the backfill may influence the operation of the heater because temperatures greater than 2,000°C may exceed the temperature rating of conventional heater components.*

A.1.3 Effects of Latent Heat on Temperature Distributions

The latent heats of various rocks are not well documented, but McBirney [1984] indicates a range between 271,000 J/kg and 419,000 J/kg. How the latent heat is consumed across the melting phase (e.g., the latent heat energy may be dispersed over a range of temperature as different minerals melt) is even more uncertain. Gibb et al. [2008] assumed a latent heat value of 300,000 J/kg and that the latent heat is entirely consumed at either the solidus or liquidus temperatures. The results of Gibb et al. [2008] suggest that the maximum temperatures attained at the borehole wall and 0.4 m into the host rock vary by less than 1 percent, assuming the latent heat was entirely consumed at either the solidus or liquidus temperatures. However, the time it took for the borehole wall to reach maximum temperature increased by 10 percent when the latent heat was consumed at the solidus temperature compared to the time it took when the latent heat was consumed at the liquidus temperature. To determine the impact that variations in latent heat values may have on the temperature distribution and the power requirements for the conceptual heater design, additional simulations were performed by assuming latent heat values of 271,000 J/kg, 300,000 J/kg, and 419,000 J/kg. In the simulations, the latent heat was evenly distributed over the entire melting range with the solidus occurring at 700°C and the liquidus at 900°C. This assumption allows the temperature of the partial melt to increase although the entire latent heat has not been consumed.

The effect that latent heat has on the predicted temperature distribution is illustrated in Figures A-5 through A-8. Figure A-5 presents the borehole wall temperature predicted at the midheight of the heater as a function of time, while Figure A-6 presents the rock temperature at a radial distance of 10 cm from the borehole wall as a function of time. The predicted temperatures increase rapidly but become nearly constant after short periods of time. At each location the latent heat values did not have a significant effect on the long-term borehole wall temperatures, but the values of latent heat do have a slight impact on the time required to attain similar temperatures. Borehole wall temperatures exceeding 800°C are predicted shortly after 36 hours, assuming latent heat values of 271,000 J/kg, 300,000 J/kg, and 419,000 J/kg. However, borehole wall temperatures of 800°C at a radial distance of 10 cm from the borehole wall (Figure A-6) were not predicted until approximately 6 days and 8 day for latent heat values

RSI-2492-15-022

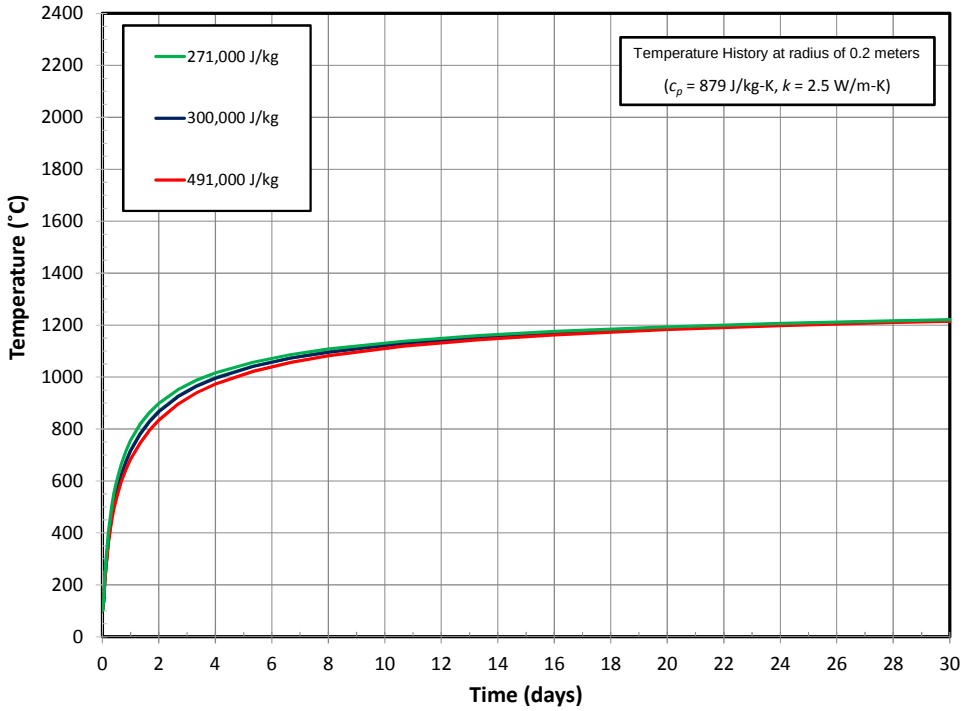

Figure A-5. Borehole Wall Temperature Versus Time Predicted at the Heater Midheight for Different Latent Heats.

RSI-2492-15-023

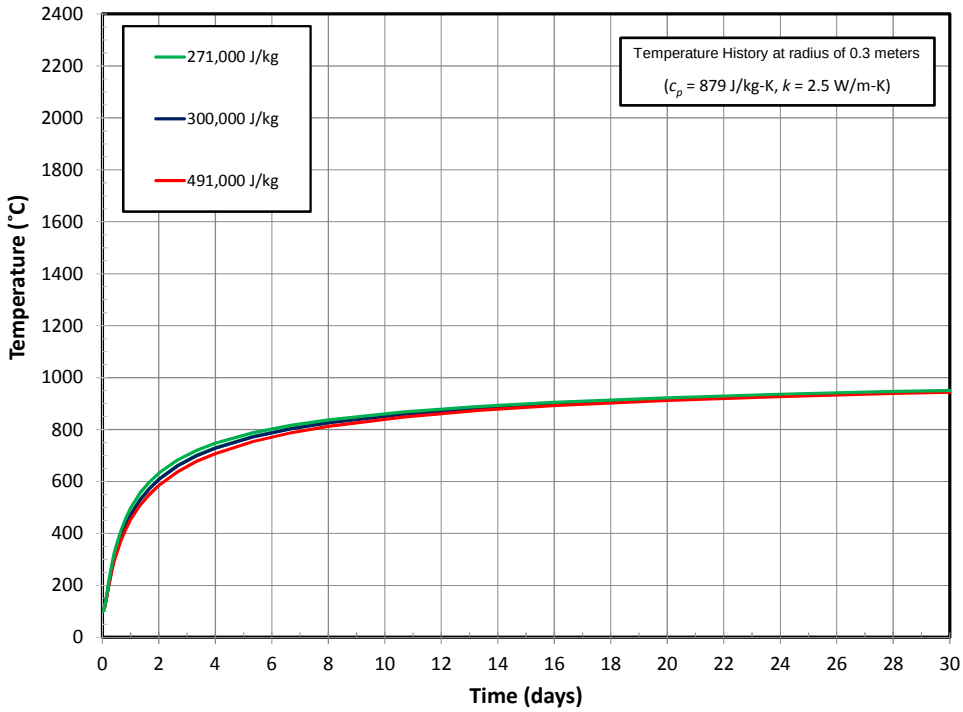

Figure A-6. Rock Temperature Predicted 10 Centimeters From the Borehole Wall Versus Time for Different Latent Heats.

of 271,000 J/kg and 419,000 J/kg, respectively.

Figures A-7 and A-8 present the rock temperature predicted at 32 days as a function of radial (Figure A-7) and axial (Figure A-8) distance from the heater for the different latent heat values evaluated. At 32 days, the borehole wall temperature at the midheight of the heater (Figure A-7) was approximately 1,150°C, regardless of the latent heat value. The predicted temperature distributions also reveal temperatures greater than 800°C extend approximately 15 cm radially from the borehole wall and approximately 17 cm axially from the base of the heater. *These results suggest partial melts of the backfill may occur as soon as 2 days, but it may take longer than 8 days to achieve partial melts 10 cm into the host rock and even after 30 days, temperatures greater than 800˚C are limited to radial distances less than 15 cm from the borehole wall and axial distances less than 17 cm from the base of the heater.*

A.2 HEAT TRANSFER FINITE ELEMENT PROGRAM

The two-dimensional, finite element heat transfer program **SPECTROM-41** [Svalstad, 1989] was developed by RESPEC to analyze thermal problems in geological formations. The primary transport process modeled by **SPECTROM-41** is conductive heat transfer. **SPECTROM-41** has the capability to model complex material properties (including temperature-dependent thermal conductivity) and boundary conditions and the code has been verified and validated. **SPECTROM-41** was used in this study to simulate the heat transfer between the heater, backfill, and country rock.

A.3 FINITE ELEMENT MODELS

Two axisymmetric finite element models were developed to predict the heat transfer from the conceptual heaters and to delineate the melting front. One model was an axisymmetric representation of the deep borehole concept while the second model was an axisymmetric approximation of the proposed Sanford Underground Research Facility (SURF) test site. Each model is described below.

A.3.1 Deep Borehole Model

A schematic of the axisymmetric finite element model representing a 40-cm-diameter borehole is shown in Figure A-9. The top boundary of the model represents a symmetry plane through the midheight of the heater; the bottom boundary of the model was selected to isolate the temperature distribution around the heater from the influences of the bottom boundary. The left boundary is the axis of symmetry through the center of the heater, and the right boundary is located 1,000 m from the centerline of the heater and is sufficiently removed to isolate the temperature distributions from the influence of the right boundary. The boundary conditions specified along the sides of the axisymmetric model assume the initial temperature conditions and are insulated; thus, no heat is transferred across the boundaries. The regions immediately

RSI-2492-15-024

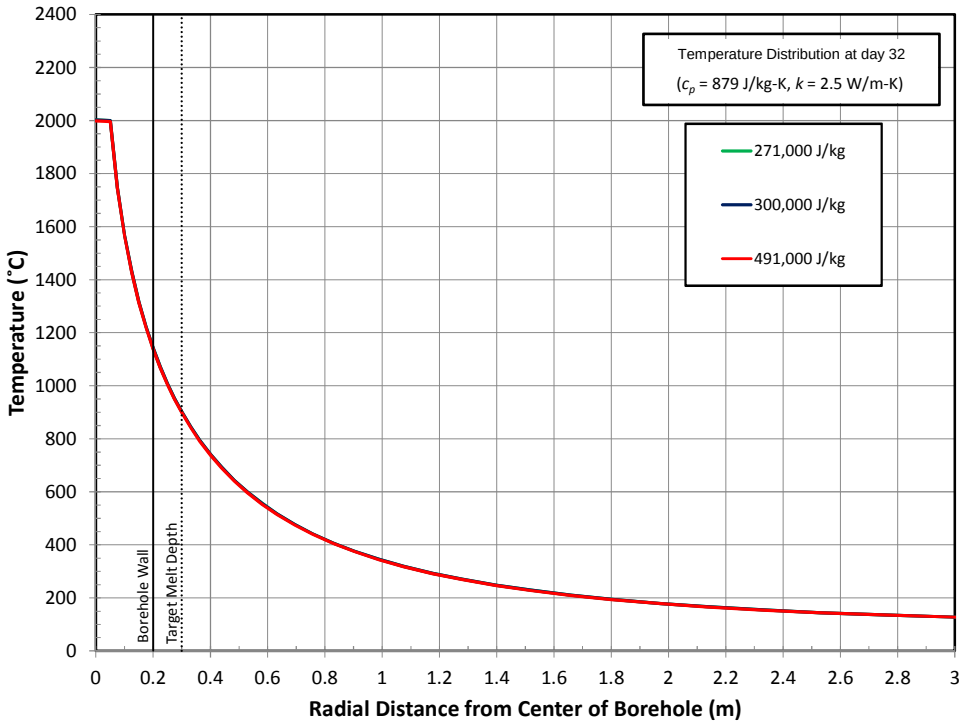

Figure A-7. Temperature Versus Radial Distance Predicted at the Heater Midheight at 32 Days for Different Latent Heats.

RSI-2492-15-025

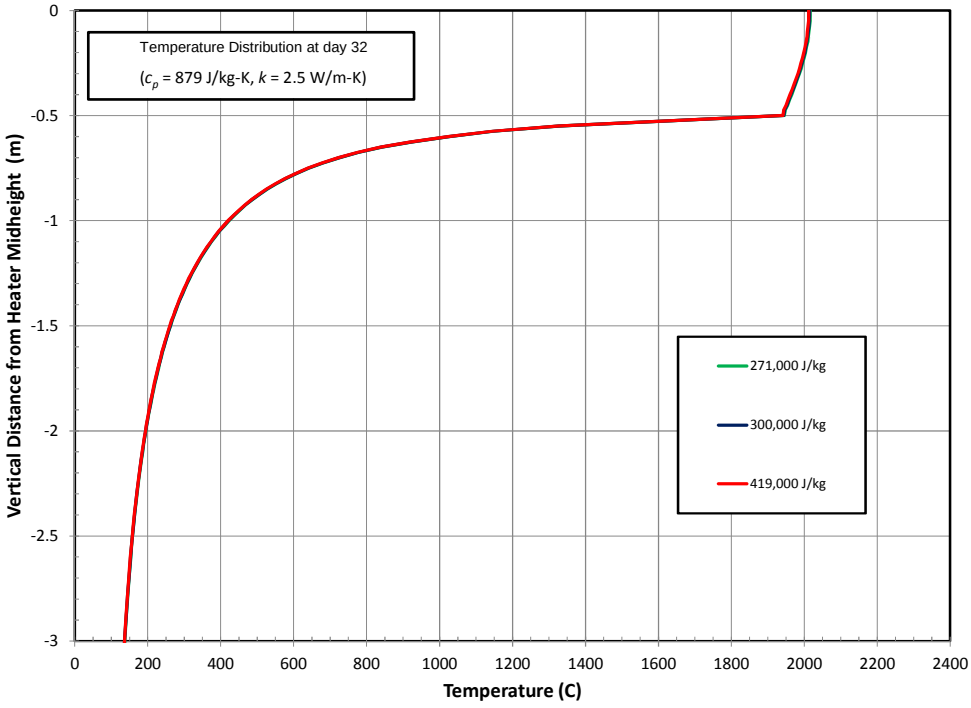

Figure A-8. Temperature Versus Axial Distance From the Heater Midheight Predicted for Different Latent Heats at 32 Days.

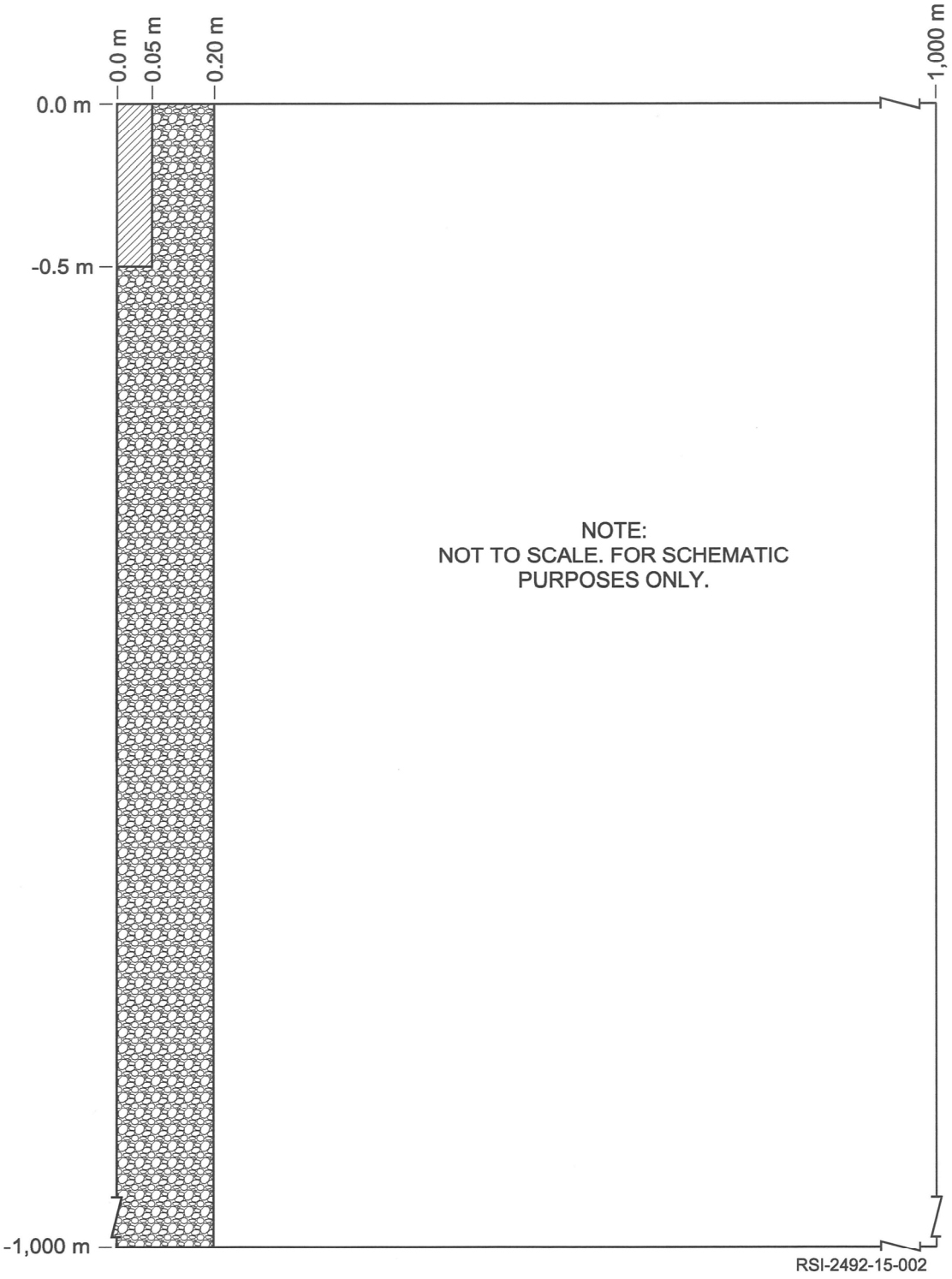

Figure A-9. Schematic Illustrating the Numerical Model Representing the Deep Borehole Disposal Concept.

outside the borehole wall are very finely subdivided to accurately represent the high-temperature gradients that are anticipated near the borehole wall. These boundary conditions represent a single isolated heater that is 1 m in length and 10 cm in diameter. For modeling purposes, the backfill material within the borehole was assumed to extend the entire height of the model. The finite element mesh of the borehole model contains 14,049 nodes and 4,590 eight-noded elements.

A.3.2 Sanford Underground Research Facility Model

A schematic of the axisymmetric approximation of the proposed SURF test site is shown in Figure A-10. The top boundary of the model represents a symmetry plane through the midheight of the heater, which is also assumed to be located midheight between two mine levels. The bottom boundary of the model was selected to isolate the temperature distribution around the heater from the influences of the bottom boundary. The left boundary is the axis of symmetry through the center of the heater, and the right boundary is located 500 m from the centerline of the heater. The boundary conditions specified along the outer limits of the axisymmetric model assume the initial temperature conditions and are insulated, thus, no heat is transferred across the boundaries. The regions immediately outside the borehole wall are very finely subdivided to accurately represent the high-temperature gradients that are anticipated near the borehole wall. Also represented in the model is a 2.75-m (9-ft) high drift located 45.72 m (150 ft) from the midheight of the heater. For modeling purposes, the backfill material within the borehole was assumed to only extend 1.5 m below the heater; the remaining borehole and excavation are assumed to be filled with air. The finite element mesh of the borehole model contains 16,813 nodes and 5,504 eight-noded elements.

A.4 REFERENCES

Gibb, F. G. G., N. A. McTaggart, K. P. Travis, and D. Burley, 2008b. "A Model for Heat Flow in Deep Borehole Disposals of High-Level Nuclear Waste," *J. Geophys. Res.*, vol. 113, Issue B5.

McBirney, A. R. 1984. *Igneous Petrology*, Freeman, San Francisco, CA.

Robertson, E. C., 1988. *Thermal Properties of Rocks*, Open-File Report 88-441, prepared by the United States Department of the Interior Geological Survey, Reston, VA.

Robertson, E. C. and D. L. Peck, 1974. "Thermal Conductivity of Vesicular Basalt From Hawaii," *Journal of Geophysical Research*, Vol. 79, pp. 4875–4888.

Svalstad, D. K., 1989. *Documentation of SPECTROM-41: A Finite Element Heat Transfer Analysis Program*, DOE/CH/10378-1, prepared by RESPEC, Rapid City, SD, for the U.S. Department of Energy, Chicago Operations Office, Argonne, IL.

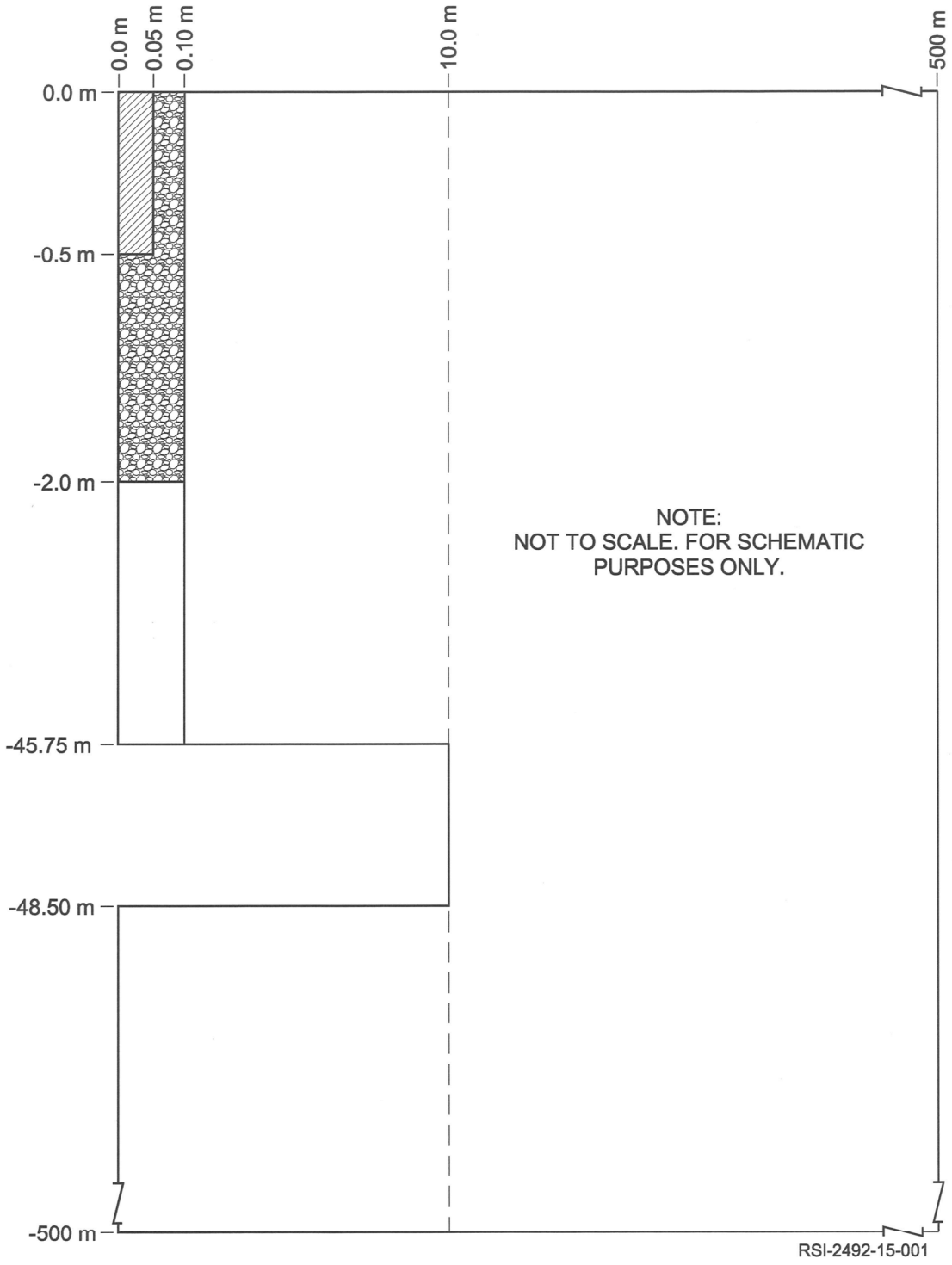

Figure A-10. Schematic Illustrating the Numerical Model Representing the In Situ Melting Experiment at the Sanford Underground Research Facility.

APPENDIX B

LABORATORY TESTING

APPENDIX B
LABORATORY TESTING

Laboratory testing was performed to determine the thermal properties, the melting temperature, and the mineralogy of the proposed host rock for a field-scale test at the Sanford Underground Research Facility (SURF). The laboratory tests and melting experiments were conducted on rock samples obtained from the 1700 Level near the Ross Shaft Station. The thermal property and mineralogy testing was performed by RESPEC at its laboratory in Rapid City, South Dakota. The melting experiments were carried out under the guidance of Dr. Stanley Howard at the South Dakota School of Mines & Technology in Rapid City, South Dakota. The following sections describe the laboratory procedures and the results of the thermal property testing and melting experiments.

B.1 THERMAL PROPERTY TESTING

To accurately calculate temperature distributions throughout the rock at SURF as a function of time and to calculate the energy required to raise the country rock to the melting temperature, site-specific thermal properties are required. These thermal properties can be classified as a material transport property or a material thermodynamic property. The transport properties include thermal conductivity (k) and thermal diffusivity (α). Thermal conductivity is a measure of the rock's ability to conduct heat, while thermal diffusivity measures the ability of a rock to conduct thermal energy relative to its ability to store thermal energy. Rocks with large thermal diffusivity will respond quickly to changes in the thermal environment, while material with small thermal diffusivity values will respond more slowly and take longer to reach equilibrium. The material thermodynamic properties include specific heat (c_p) and volumetric heat capacity. Specific heat is defined as the energy required to raise the temperature of a unit mass by 1 degree and volumetric heat capacity measures the ability of a material to store thermal energy and is the product of the material density and specific heat.

B.1.1 Procedure

Test samples of rhyolite and Ellison rock were obtained from the 1700 Level at SURF. Tests were performed in accordance with the recommended procedures for the Thermtest system used for determining thermal properties. For the thermal tests, the specimens were cut in half and one face on each half was finished flat. Figures B-1 and B-2 illustrate photographs of the rhyolite and Ellison test specimens, respectively. The thickness of each half was greater than 25 millimeters (mm) to isolate the test from losses that will occur on the unfinished surfaces of the specimens. The test specimens were placed in an oven with the sensor positioned between the two finished surfaces. The oven was brought to the specified test temperature and allowed to stabilize before initiating the test. When the sample temperature inside the oven was stable, a predetermined power of 0.1 W was supplied to the heater, and the sensor positioned between the two finished surfaces measured the temperature change as it radiated outward from the

Figure B-1. Rhyolite Sample Obtained From the Sanford Underground Research Facility Near the 1700 Level Ross Shaft Station.

Figure B-2. Ellison Sample Obtained From the Sanford Underground Research Facility Near the 1700 Level Ross Shaft Station.

center. The rate of temperature change (measured by the sensor) through the sample was used to calculate values of thermal conductivity and thermal diffusivity internally by the Thermtest system and software. Values for specific heat (c_p) could then be determined indirectly based on the calculated volumetric heat capacity; which in turn, is the ratio of measured thermal conductivity value to the measured thermal diffusivity value.

B.1.2 Results

Thermal properties for the rhyolite and Ellison specimens were initially determined at room temperature (20°C), and the temperature dependence of the thermal properties was assessed by performing tests at intervals of 28°C beginning at 38°C and concluding at 262°C, which was the maximum temperature of the oven. The thermal conductivity values of the rhyolite ranged from a high of 2.54 Watts per kilogram Kelvin (W/kg-K) at a temperature 20°C to a low of 2.13 W/kg-K at a temperature of 262°C. Similarly, the thermal conductivity values of the Ellison ranged from a high of 1.58 W/kg-K at a temperature 20°C to a low of 1.27 W/kg-K at a temperature of 262°C. These results are consistent with the generally expected behavior of rocks—thermal conductivity values decrease with increasing temperature. Furthermore, at these relatively low temperatures, the thermal conductivity value's dependence on temperature appears nearly linear.

The values of volumetric heat capacity for the intact specimens are also consistent with the generally expected behavior of rocks where the volumetric heat capacity increases as the temperature increases. The volumetric heat capacity values of the rhyolite ranged from a low of 1.724 mega Joules per cubic meter Kelvin (MJ/m^3-K) at a temperature 20°C to a high of 2.420 MJ/m^3-K at a temperature of 262°C. Similarly, the volumetric heat capacity values of the Ellison ranged from a low of 0.616 MJ/m^3-K at a temperature 20°C to a high of 0.946 MJ/m^3-K at a temperature of 262°C. Figures B-3 and B-4 graphically illustrate the temperature dependence of thermal conductivity and specific heat values for the tested specimens at each temperature and the entire dataset is provided in Tables B-1 and B-2 for the rhyolite and Ellison tests, respectively.

In addition to determining thermal properties for an intact rhyolite specimen, the impact that backfill porosity has on the thermal properties was also determined by conducting tests on three crushed samples of the rhyolite corresponding to porosities of approximately 44 percent, 39 percent, and 27 percent. The thermal conductivity values obtained from the dry samples of crushed rhyolite are also illustrated in Figure B-3. The measured thermal conductivity values are significantly less than those determined for the intact rhyolite and are similar for each porosity value with slightly greater values determined for lower porosity values. The thermal conductivity values ranged from a low of 0.23 W/kg-K at a temperature 20°C to a high of 0.39 W/kg-K at a temperature of 262°C. These results exhibit an opposite trend, which indicates that the thermal conductivity of the backfill increases with increased temperature. The thermal conductivity values determined for the crushed rhyolite are consistent with thermal conductivity values of dry sand, which typically range between 0.15 W/m-K to 0.25 W/m-K. The measured values of volumetric heat capacity for the crushed rhyolite (Figure B-4) were also

RSI-2492-15-028

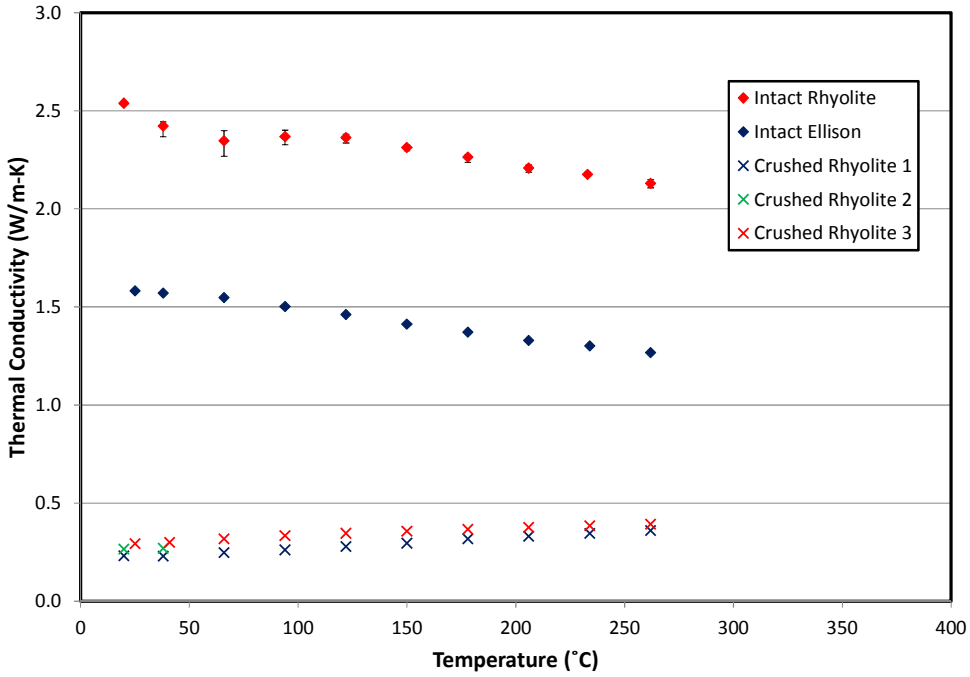

Figure B-3. Laboratory Results of Thermal Conductivity Tests Performed on the Rhyolite and Ellison Samples.

RSI-2492-15-029

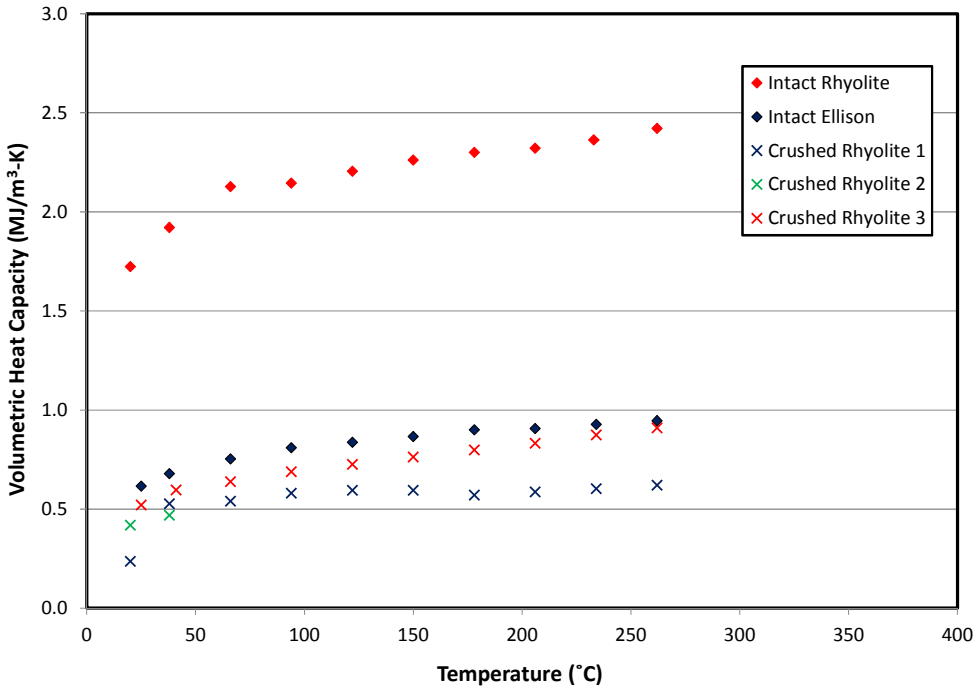

Figure B-4. Laboratory Results of Specific Heat Tests Performed on the Rhyolite and Ellison Samples.

Table B-1. Results of Thermal Property Testing of Intact Rhyolite (Page 1 of 3)

Rhyolite 4-15	Temperature (°C)	Thermal Conductivity (W/m-K)	Thermal Diffusivity (10^{-6} m^2/s)	Volumetric Heat Capacity (MJ/m^3-K)
Test 1	20.0	2.5452	1.4851	1.7139
Test 2	20.0	2.5428	1.4651	1.7356
Test 3	20.0	2.5398	1.4867	1.7083
Test 4	20.0	2.5353	1.4638	1.7320
Test 5	20.0	2.5327	1.4635	1.7306
Average		**2.5391**	**1.4728**	**1.7241**
Standard Deviation		**0.0052**	**0.0120**	**0.0122**
Test 1	38.0	2.3675	1.2129	1.9519
Test 2	38.0	2.4391	1.3429	1.8164
Test 3	38.0	2.4143	1.2404	1.9463
Test 4	38.0	2.4414	1.2455	1.9602
Test 5	38.0	2.4427	1.2644	1.9319
Average		**2.4210**	**1.2612**	**1.9213**
Standard Deviation		**0.0321**	**0.0492**	**0.0596**
Test 1	66.0	2.2677	0.9888	2.2933
Test 2	66.0	2.3219	1.0508	2.2097
Test 3	66.0	2.3632	1.1419	2.0696
Test 4	66.0	2.3844	1.1595	2.0564
Test 5	66.0	2.3978	1.1914	2.0127
Average		**2.3470**	**1.1065**	**2.1283**
Standard Deviation		**0.0529**	**0.0840**	**0.1181**
Test 1	94.0	2.3266	1.0610	2.1929
Test 2	94.0	2.3496	1.0888	2.1580
Test 3	94.0	2.3706	1.1149	2.1264
Test 4	94.0	2.3931	1.1163	2.1438
Test 5	94.0	2.4011	1.1403	2.1057
Average		**2.3682**	**1.1042**	**2.1453**
Standard Deviation		**0.0308**	**0.0303**	**0.0330**

Table B-1. Results of Thermal Property Testing of Intact Rhyolite (Page 2 of 3)

Rhyolite 4-15	Temperature (°C)	Thermal Conductivity (W/m-K)	Thermal Diffusivity (10^{-6} m^2/s)	Volumetric Heat Capacity (MJ/m^3-K)
Test 1	122.0	2.3354	1.0315	2.2640
Test 2	122.0	2.3611	1.0675	2.2118
Test 3	122.0	2.3617	1.0683	2.2106
Test 4	122.0	2.3765	1.0807	2.1990
Test 5	122.0	2.3811	1.1138	2.1378
Average		**2.3632**	**1.0724**	**2.2047**
Standard Deviation		**0.0179**	**0.0296**	**0.0450**
Test 1	150.0	2.2963	1.0351	2.2184
Test 2	150.0	2.3041	1.0159	2.2680
Test 3	150.0	2.3117	1.0089	2.2913
Test 4	150.0	2.3243	1.0259	2.2657
Test 5	150.0	2.3235	1.0251	2.2666
Average		**2.3120**	**1.0222**	**2.2620**
Standard Deviation		**0.0122**	**0.0101**	**0.0266**
Test 1	178.0	2.2376	0.9367	2.3887
Test 2	178.0	2.2757	1.0249	2.2203
Test 3	178.0	2.2656	0.9856	2.2986
Test 4	178.0	2.2701	0.9883	2.2970
Test 5	178.0	2.2729	0.9896	2.2967
Average		**2.2644**	**0.9850**	**2.3003**
Standard Deviation		**0.0154**	**0.0315**	**0.0597**
Test 1	206.0	2.1870	0.9187	2.3805
Test 2	206.0	2.2074	0.9629	2.2923
Test 3	206.0	2.2230	0.9791	2.2705
Test 4	206.0	2.2135	0.9497	2.3307
Test 5	206.0	2.2075	0.9461	2.3332
Average		**2.2077**	**0.9513**	**2.3214**
Standard Deviation		**0.0132**	**0.0224**	**0.0423**

Table B-1. Results of Thermal Property Testing of Intact Rhyolite (Page 3 of 3)

Rhyolite 4-15	Temperature (°C)	Thermal Conductivity (W/m-K)	Thermal Diffusivity (10^{-6} m^2/s)	Volumetric Heat Capacity (MJ/m^3-K)
Test 1	234.0	2.1673	0.9037	2.3983
Test 2	234.0	2.1749	0.9153	2.3763
Test 3	234.0	2.1697	0.9184	2.3625
Test 4	234.0	2.1869	0.9430	2.3190
Test 5	234.0	2.1766	0.9210	2.3634
Average		**2.1751**	**0.9203**	**2.3639**
Standard Deviation		**0.0076**	**0.0143**	**0.0290**
Test 1	262.0	2.1076	0.8552	2.4644
Test 2	262.0	2.1210	0.8780	2.4157
Test 3	262.0	2.1489	0.8991	2.3900
Test 4	262.0	2.1343	0.8802	2.4249
Test 5	262.0	2.1378	0.8873	2.4094
Average		**2.1299**	**0.8800**	**2.4209**
Standard Deviation		**0.0160**	**0.0161**	**0.0275**

significantly lower than those values determined for the intact rock but exhibit a similar trend where the values of volumetric heat capacity increase with increasing temperature. The volumetric heat capacity values of the crushed rhyolite ranged from a low of 0.24 MJ/m^3-K at a temperature 20°C to a high of 0.91 MJ/m^3-K at a temperature of 262°C. Tables B-3 through B-5 provide the laboratory results of thermal tests performed on the three crushed samples of rhyolite.

B.2 ROCK MELT TESTS

Attrill and Gibb [2003] have previously performed melting experiments to characterize the partial melting temperature of typical crustal granites. The specimens of granite were obtained from the Caledonian age from the North of England. The results of the experiments revealed partial melting of the granite rock can be achieved at temperatures between 700°C and 800°C; however, these experiments were carried out under conditions expected in the environment of a deep borehole disposal system. The experiments were conducted at pressures greater than 0.15 GPa and water concentrations between 0 percent and 5 percent weight, which is known to significantly reduce the melting temperatures. Therefore, additional melting experiments were carried out at the South Dakota School of Mines & Technology to determine the melting temperatures of rhyolite under dry conditions.

Table B-2. Results of Thermal Property Testing of Intact Ellison (Page 1 of 3)

Ellison 4-10	Temperature (°C)	Thermal Conductivity (W/m-K)	Thermal Diffusivity (10^{-6} m^2/s)	Volumetric Heat Capacity (MJ/m^3-K)
Test 1	20.0	1.5797	2.6355	0.5994
Test 2	20.0	1.5838	2.6145	0.6058
Test 3	20.0	1.5790	2.6197	0.6027
Test 4	20.0	1.5868	2.6055	0.6090
Test 5	20.0	1.5830	2.3798	0.6652
Average		**1.5825**	**2.5710**	**0.6164**
Standard Deviation		**0.0032**	**0.1075**	**0.0275**
Test 1	38.0	1.5686	2.4022	0.6530
Test 2	38.0	1.5687	2.2578	0.6948
Test 3	38.0	1.5725	2.2730	0.6918
Test 4	38.0	1.5719	2.3303	0.6745
Average		**1.5704**	**2.3158**	**0.6785**
Standard Deviation		**0.0021**	**0.0655**	**0.0192**
Test 1	66.0	1.5419	2.0517	0.7515
Test 2	66.0	1.5473	2.0422	0.7577
Test 3	66.0	1.5507	2.0501	0.7564
Test 4	66.0	1.5478	2.0631	0.7502
Test 5	66.0	1.5492	2.0674	0.7494
Average		**1.5474**	**2.0549**	**0.7530**
Standard Deviation		**0.0034**	**0.0102**	**0.0038**
Test 1	94.0	1.4939	1.8227	0.8196
Test 2	94.0	1.5009	1.8660	0.8044
Test 3	94.0	1.5034	1.8665	0.8055
Test 4	94.0	1.5044	1.8556	0.8108
Test 5	94.0	1.5063	1.8611	0.8094
Average		**1.5018**	**1.8544**	**0.8099**
Standard Deviation		**0.0048**	**0.0182**	**0.0060**

Table B-2. Results of Thermal Property Testing of Intact Ellison (Page 2 of 3)

Ellison 4-10	Temperature (°C)	Thermal Conductivity (W/m-K)	Thermal Diffusivity (10^{-6} m^2/s)	Volumetric Heat Capacity (MJ/m^3-K)
Test 1	122.0	1.4542	1.7024	0.8542
Test 2	122.0	1.4562	1.7483	0.8329
Test 3	122.0	1.4646	1.7547	0.8347
Test 4	122.0	1.4616	1.7519	0.8343
Test 5	122.0	1.4647	1.7624	0.8311
Average		**1.4603**	**1.7440**	**0.8374**
Standard Deviation		**0.0048**	**0.0238**	**0.0095**
Test 1	150.0	1.4068	1.6013	0.8785
Test 2	150.0	1.4135	1.6613	0.8508
Test 3	150.0	1.4127	1.6277	0.8679
Test 4	150.0	1.4174	1.6288	0.8702
Test 5	150.0	1.4118	1.6259	0.8683
Average		**1.4124**	**1.6290**	**0.8672**
Standard Deviation		**0.0038**	**0.0213**	**0.0101**
Test 1	178.0	1.3683	1.5000	0.9122
Test 2	178.0	1.3712	1.5243	0.8996
Test 3	178.0	1.3726	1.5295	0.8974
Test 4	178.0	1.3739	1.5336	0.8959
Test 5	178.0	1.3751	1.5283	0.8997
Average		**1.3722**	**1.5231**	**0.9010**
Standard Deviation		**0.0026**	**0.0134**	**0.0065**
Test 1	206.0	1.3233	1.4405	0.9186
Test 2	206.0	1.3316	1.4482	0.9195
Test 3	206.0	1.3329	1.4565	0.9152
Test 4	206.0	1.3251	1.5324	0.8647
Test 5	206.0	1.3353	1.4560	0.9171
Average		**1.3296**	**1.4667**	**0.9070**
Standard Deviation		**0.0052**	**0.0373**	**0.0237**

Table B-2. Results of Thermal Property Testing of Intact Ellison (Page 3 of 3)

Ellison 4-10	Temperature (°C)	Thermal Conductivity (W/m-K)	Thermal Diffusivity (10^{-6} m^2/s)	Volumetric Heat Capacity (MJ/m^3-K)
Test 1	234.0	1.2990	1.3691	0.9488
Test 2	234.0	1.2937	1.4711	0.8794
Test 3	234.0	1.3030	1.3938	0.9349
Test 4	234.0	1.3067	1.3885	0.9411
Test 5	234.0	1.3059	1.3964	0.9352
Average		**1.3017**	**1.4038**	**0.9279**
Standard Deviation		**0.0054**	**0.0391**	**0.0277**
Test 1	262.0	1.2618	1.3244	0.9527
Test 2	262.0	1.2700	1.3419	0.9464
Test 3	262.0	1.2649	1.3401	0.9439
Test 4	262.0	1.2695	1.3457	0.9434
Test 5	262.0	1.2661	1.3402	0.9447
Average		**1.2665**	**1.3385**	**0.9462**
Standard Deviation		**0.0034**	**0.0082**	**0.0038**

B.2.1 Procedure

Induction heating was used determine the melting temperature of samples of rhyolite obtained at SURF near the 1700 Level Ross Shaft Station. Induction heating is a process of heating an electrically conducting material by electromagnetic induction. For these experiments, the eddy currents resulting from the electromagnetic induction were generated within a graphite crucible and the resistance leads to Joule heating of the crucible. The heat is then transferred to the test sample by radiation and conduction; during the tests, the sample temperature was indirectly measured by placing a molybdenum thermocouple into a vertically machined hole located in the sidewall of the crucible.

Particle sizes of the crushed samples varied between 250 micrometers (µm) and 425 µm. The crushed samples were placed in a ceramic liner that was then inserted into a machined graphite crucible that had previously been fired at 1,800°C. The sample, liner, and crucible were then weighed before being placed in a glass tube with insulation packed above and below the crucible to reduce heat loss. The entire assembly was then placed into the induction coils. During all of the melting experiments, argon gas was flushed through the glass tube to suppress oxidation. Before applying power to the induction heater, argon gas was flushed through the system to approximate the convection coefficient. After approximately 3 minutes, the power of the

Table B-3. Results of Thermal Property Testing of Crushed Rhyolite Sample 1[a] (Page 1 of 4)

Rhyolite 4-15	Temperature (°C)	Thermal Conductivity (W/m-K)	Thermal Diffusivity (10^{-6} m^2/s)	Volumetric Heat Capacity (MJ/m^3-K)
Test 1	20.0	0.2300	0.9782	0.2352
Test 2	20.0	0.2329	0.9996	0.2330
Test 3	20.0	0.2329	0.9948	0.2341
Test 4	20.0	0.2341	1.0007	0.2340
Test 5	20.0	0.2333	1.0002	0.2333
Average		**0.2315**	**0.9800**	**0.2364**
Standard Deviation		**0.0022**	**0.0327**	**0.0065**
Test 1	38.0	0.2306	0.4438	0.5195
Test 2	38.0	0.2232	0.4083	0.5468
Test 3	38.0	0.2321	0.4241	0.5473
Test 4	38.0	0.2319	0.4644	0.4993
Test 5	38.0	0.2281	0.4358	0.5234
Average		**0.2292**	**0.4353**	**0.5273**
Standard Deviation		**0.0037**	**0.0211**	**0.0203**
Test 1	66.0	0.2489	0.4663	0.5338
Test 2	66.0	0.2509	0.4712	0.5324
Test 3	66.0	0.2465	0.4528	0.5444
Test 4	66.0	0.2413	0.4316	0.5591
Test 5	66.0	0.2509	0.4715	0.5321
Average		**0.2477**	**0.4587**	**0.5403**
Standard Deviation		**0.0040**	**0.0169**	**0.0116**
Test 1	94.0	0.2647	0.4676	0.5661
Test 2	94.0	0.2533	0.3994	0.6343
Test 3	94.0	0.2652	0.4712	0.5628
Test 4	94.0	0.2615	0.4515	0.5793
Test 5	94.0	0.2657	0.4726	0.5623
Average		**0.2621**	**0.4525**	**0.5809**
Standard Deviation		**0.0052**	**0.0308**	**0.0306**

Table B-3. Results of Thermal Property Testing of Crushed Rhyolite Sample 1[(a)] (Page 2 of 4)

Rhyolite 4-15	Temperature (°C)	Thermal Conductivity (W/m-K)	Thermal Diffusivity (10^{-6} m^2/s)	Volumetric Heat Capacity (MJ/m^3-K)
Test 1	122.0	0.2809	0.4786	0.5870
Test 2	122.0	0.2788	0.4692	0.5942
Test 3	122.0	0.2716	0.4418	0.6149
Test 4	122.0	0.2817	0.4774	0.5901
Test 5	122.0	0.2814	0.4790	0.5874
Average		**0.2789**	**0.4692**	**0.5947**
Standard Deviation		**0.0042**	**0.0158**	**0.0116**
Test 1	150.0	0.2943	0.4799	0.6132
Test 2	150.0	0.2956	0.4835	0.6115
Test 3	150.0	0.2944	0.4797	0.6138
Test 4	150.0	0.2866	0.4463	0.6420
Test 5	150.0	0.2945	0.4766	0.6179
Average		**0.2961**	**0.5034**	**0.5957**
Standard Deviation		**0.0081**	**0.0752**	**0.0600**
Test 1	178.0	0.3200	0.6361	0.5031
Test 2	178.0	0.3010	0.4502	0.6686
Test 3	178.0	0.3263	0.6599	0.4945
Test 4	178.0	0.3099	0.4857	0.6379
Test 5	178.0	0.3255	0.6563	0.4960
Test 6	178.0	0.3088	0.4813	0.6417
Test 7	178.0	0.3287	0.6657	0.4937
Test 8	178.0	0.3125	0.4921	0.6352
Test 9	178.0	0.3283	0.6668	0.4923
Test 10	178.0	0.3118	0.4890	0.6377
Average		**0.3173**	**0.5683**	**0.5701**
Standard Deviation		**0.0097**	**0.0945**	**0.0787**

Table B-3. Results of Thermal Property Testing of Crushed Rhyolite Sample 1[(a)] (Page 3 of 4)

Rhyolite 4-15	Temperature (°C)	Thermal Conductivity (W/m-K)	Thermal Diffusivity (10^{-6} m^2/s)	Volumetric Heat Capacity (MJ/m^3-K)
Test 1	206.0	0.3411	0.6682	0.5105
Test 2	206.0	0.3247	0.4943	0.6569
Test 3	206.0	0.3409	0.6712	0.5079
Test 4	206.0	0.3243	0.4948	0.6555
Test 5	206.0	0.3400	0.6651	0.5112
Test 6	206.0	0.3229	0.4876	0.6621
Test 7	206.0	0.3340	0.6377	0.5238
Test 8	206.0	0.3157	0.4635	0.6811
Test 9	206.0	0.3418	0.6725	0.5083
Test 10	206.0	0.3256	0.4985	0.6530
Average		**0.3311**	**0.5753**	**0.5871**
Standard Deviation		**0.0096**	**0.0933**	**0.0792**
Test 1	234.0	0.3548	0.6747	0.5259
Test 2	234.0	0.3381	0.4998	0.6764
Test 3	234.0	0.3482	0.6485	0.5370
Test 4	234.0	0.3298	0.4739	0.6960
Test 5	234.0	0.3551	0.6754	0.5258
Test 6	234.0	0.3378	0.4962	0.6807
Test 7	234.0	0.3567	0.6777	0.5264
Test 8	234.0	0.3405	0.5059	0.6730
Test 9	234.0	0.3561	0.6813	0.5227
Test 10	234.0	0.3396	0.5053	0.6720
Average		**0.3457**	**0.5839**	**0.6036**
Standard Deviation		**0.0097**	**0.0932**	**0.0805**

Table B-3. Results of Thermal Property Testing of Crushed Rhyolite Sample 1[a] (Page 4 of 4)

Rhyolite 4-15	Temperature (°C)	Thermal Conductivity (W/m-K)	Thermal Diffusivity (10^{-6} m^2/s)	Volumetric Heat Capacity (MJ/m^3-K)
Test 1	262.0	0.3697	0.6815	0.5425
Test 2	262.0	0.3522	0.5032	0.7000
Test 3	262.0	0.3714	0.6867	0.5409
Test 4	262.0	0.3547	0.5125	0.6921
Test 5	262.0	0.3698	0.6837	0.5410
Test 6	262.0	0.3532	0.5109	0.6913
Test 7	262.0	0.3719	0.6899	0.5391
Test 8	262.0	0.3552	0.5129	0.6925
Test 9	262.0	0.3624	0.6555	0.5528
Test 10	262.0	0.3439	0.4805	0.7157
Average		**0.3604**	**0.5917**	**0.6208**
Standard Deviation		**0.0099**	**0.0934**	**0.0821**

(a) Porosity of approximately 44 percent.

induction heater was slowly increased to obtain a temperature between 200°C and 300°C to allow a gradual breakdown of any trapped water in the sample. After this initial heating, the power was incrementally increased to reach the specified test temperature, which was maintained within ± 0.5°C for approximately 20 minutes before the power to the induction heater was cut and the sample was allowed to slowly cool. After removing the crucible from the assembly, the crucible, liner, and melt were reweighed to check for any loss of material during the experiment. Finally, the liner was removed from the crucible, a polished thin section was made, and a sample of the melt was obtained for X-Ray Diffraction (XRD) analysis.

B.2.2 Results

Five induction melting experiments were performed. Each melting experiment was carried out at atmospheric pressure in the absence of additional water. These test conditions were considered appropriate to obtain melting information for determining the feasibility of the in situ melting experiment at SURF. Originally, the intention was that the partial melting phases would be determined from the temperature versus time data obtained from the tests. Therefore, the initial melting experiment was incrementally increased to a temperature of 1,800°C, allowed to cool, and then increased again. After cooling, it was obvious that a full melt had been obtained, but the melting phases could not be confidently determined from the temperature versus time data. Consequently, additional experiments were conducted at

incremental temperatures to determine the melting phases by posttest visual examination of the sample. Four additional melting experiments were carried out between 1,320°C and 1,500°C to determine the approximate temperature of the liquidus. At the conclusion of the 1,320°C melting experiment, the crushed ryholite sample was still unconsolidated, which indicated that no melt had been generated. By contrast, the melting experiment performed at 1,500°C resulted in an amalgamated mass. Subsequent melting experiments performed at 50°C intervals revealed that the partial melting temperature of rhyolite begins between 1,400°C and 1,450°C and the liquidus occurs below 1,500°C. Figure B-5 compares each of the posttest samples, and Figures B-6 through B-8 show posttest samples after being heated to temperatures of 1,320°C, 1,400°C, and 1,450°C, respectively.

Table B-4. Results of Thermal Property Testing of Crushed Rhyolite Sample[(a)] 2

Rhyolite 4-15	Temperature (°C)	Thermal Conductivity (W/m-K)	Thermal Diffusivity (10^{-6} m^2/s)	Volumetric Heat Capacity (MJ/m^3-K)
Test 1	20.0	0.2623	0.6148	0.4266
Test 2	20.0	0.2625	0.6202	0.4232
Test 3	20.0	0.2669	0.6390	0.4177
Test 4	20.0	0.2668	0.6408	0.4164
Test 5	20.0	0.2691	0.6474	0.4156
Average		**0.2659**	**0.6348**	**0.4190**
Standard Deviation		**0.0028**	**0.0139**	**0.0048**
Test 1	38.0	0.2669	0.5898	0.4526
Test 2	38.0	0.2621	0.5181	0.5060
Test 3	38.0	0.2724	0.6147	0.4431
Test 4	38.0	0.2680	0.5432	0.4934
Test 5	38.0	0.2734	0.6181	0.4423
Average		**0.2700**	**0.5800**	**0.4696**
Standard Deviation		**0.0040**	**0.0403**	**0.0272**

(a) Porosity of approximately 39 percent.

Table B-6 lists the pre- and postmelt weights for each experiment. In each of the melting experiments, a slight amount of mass was lost. The percentages varied between 0.08 percent and 0.19 percent. To determine if the mass loss was likely the loss of bound water, a sample of the crushed rhyolite was heated to 262°C. Pre- and postheating weights revealed a mass loss of approximately 0.19 percent; this result suggests that the mass lost during the melting experiments was likely attributed to the loss of bound water.

Table B-5. Results of Thermal Property Testing of Crushed Rhyolite Sample 3[(a)] (Page 1 of 3)

Rhyolite 4-15	Temperature (°C)	Thermal Conductivity (W/m-K)	Thermal Diffusivity (10^{-6} m^2/s)	Volumetric Heat Capacity (MJ/m^3-K)
Test 1	25.0	0.2933	0.4803	0.6107
Test 2	25.0	0.3002	0.5032	0.5966
Test 3	25.0	0.3030	0.5119	0.5918
Test 4	25.0	0.3038	0.5137	0.5915
Test 5	25.0	0.3036	0.5139	0.5908
Average		**0.2939**	**0.5665**	**0.5210**
Standard Deviation		**0.0138**	**0.0545**	**0.0281**
Test 1	41.0	0.2933	0.4803	0.6107
Test 2	41.0	0.3002	0.5032	0.5966
Test 3	41.0	0.3030	0.5119	0.5918
Test 4	41.0	0.3038	0.5137	0.5915
Test 5	41.0	0.3036	0.5139	0.5908
Average		**0.3008**	**0.5046**	**0.5963**
Standard Deviation		**0.0044**	**0.0143**	**0.0084**
Test 1	66.0	0.3099	0.4734	0.6546
Test 2	66.0	0.3201	0.5054	0.6335
Test 3	66.0	0.3210	0.5100	0.6293
Test 4	66.0	0.3173	0.4975	0.6377
Test 5	66.0	0.3193	0.5036	0.6340
Average		**0.3175**	**0.4980**	**0.6378**
Standard Deviation		**0.0045**	**0.0145**	**0.0098**
Test 1	94.0	0.3271	0.4611	0.7094
Test 2	94.0	0.3343	0.4855	0.6887
Test 3	94.0	0.3376	0.4978	0.6781
Test 4	94.0	0.3360	0.4921	0.6827
Test 5	94.0	0.3372	0.4936	0.6832
Average		**0.3344**	**0.4860**	**0.6884**
Standard Deviation		**0.0043**	**0.0146**	**0.0123**

Table B-5. Results of Thermal Property Testing of Crushed Rhyolite Sample 3[(a)] (Page 2 of 3)

Rhyolite 4-15	Temperature (°C)	Thermal Conductivity (W/m-K)	Thermal Diffusivity (10^{-6} m^2/s)	Volumetric Heat Capacity (MJ/m^3-K)
Test 1	122.0	0.3476	0.4841	0.7181
Test 2	122.0	0.3463	0.4775	0.7251
Test 3	122.0	0.3371	0.4520	0.7459
Test 4	122.0	0.3507	0.4881	0.7184
Test 5	122.0	0.3488	0.4849	0.7193
Average		**0.3461**	**0.4773**	**0.7254**
Standard Deviation		**0.0053**	**0.0147**	**0.0118**
Test 1	150.0	0.3558	0.4652	0.7649
Test 2	150.0	0.3476	0.4428	0.7851
Test 3	150.0	0.3596	0.4759	0.7557
Test 4	150.0	0.3613	0.4804	0.7521
Test 5	150.0	0.3587	0.4721	0.7599
Average		**0.3566**	**0.4672**	**0.7635**
Standard Deviation		**0.0054**	**0.0148**	**0.0130**
Test 1	178.0	0.3696	0.4693	0.7876
Test 2	178.0	0.3568	0.4372	0.8162
Test 3	178.0	0.3680	0.4594	0.8011
Test 4	178.0	0.3699	0.4632	0.7987
Test 5	178.0	0.3704	0.4679	0.7917
Average		**0.3670**	**0.4594**	**0.7991**
Standard Deviation		**0.0057**	**0.0130**	**0.0110**
Test 1	206.0	0.3761	0.4500	0.8357
Test 2	206.0	0.3795	0.4586	0.8275
Test 3	206.0	0.3794	0.4606	0.8236
Test 4	206.0	0.3660	0.4269	0.8573
Test 5	206.0	0.3803	0.4625	0.8223
Average		**0.3762**	**0.4517**	**0.8333**
Standard Deviation		**0.0060**	**0.0147**	**0.0144**

Table B-5. Results of Thermal Property Testing of Crushed Rhyolite Sample 3[(a)] (Page 3 of 3)

Rhyolite 4-15	Temperature (°C)	Thermal Conductivity (W/m-K)	Thermal Diffusivity (10^{-6} m^2/s)	Volumetric Heat Capacity (MJ/m^3-K)
Test 1	234.0	0.3903	0.4524	0.8627
Test 2	234.0	0.3877	0.4451	0.8712
Test 3	234.0	0.3894	0.4496	0.8660
Test 4	234.0	0.3857	0.4411	0.8744
Test 5	234.0	0.3748	0.4168	0.8992
Average		**0.3856**	**0.4410**	**0.8747**
Standard Deviation		**0.0063**	**0.0142**	**0.0144**
Test 1	262.0	0.3942	0.4376	0.9009
Test 2	262.0	0.3829	0.4090	0.9363
Test 3	262.0	0.3960	0.4400	0.9000
Test 4	262.0	0.3935	0.4327	0.9095
Test 5	262.0	0.3975	0.4413	0.9007
Average		**0.3928**	**0.4321**	**0.9095**
Standard Deviation		**0.0058**	**0.0133**	**0.0155**

(a) Porosity of approximately 27 percent.

B.3 REFERENCES

Attrill, P. G. and F. G. F. Gibb, 2003. "Partial Melting and Recrystallization of Granite and Their Application to Deep Disposal of Radioactive Waste, Part 1 – Rationale and Partial Melting," *Lithos*, 67, pp. 103–117.

RSI-2492-15-030

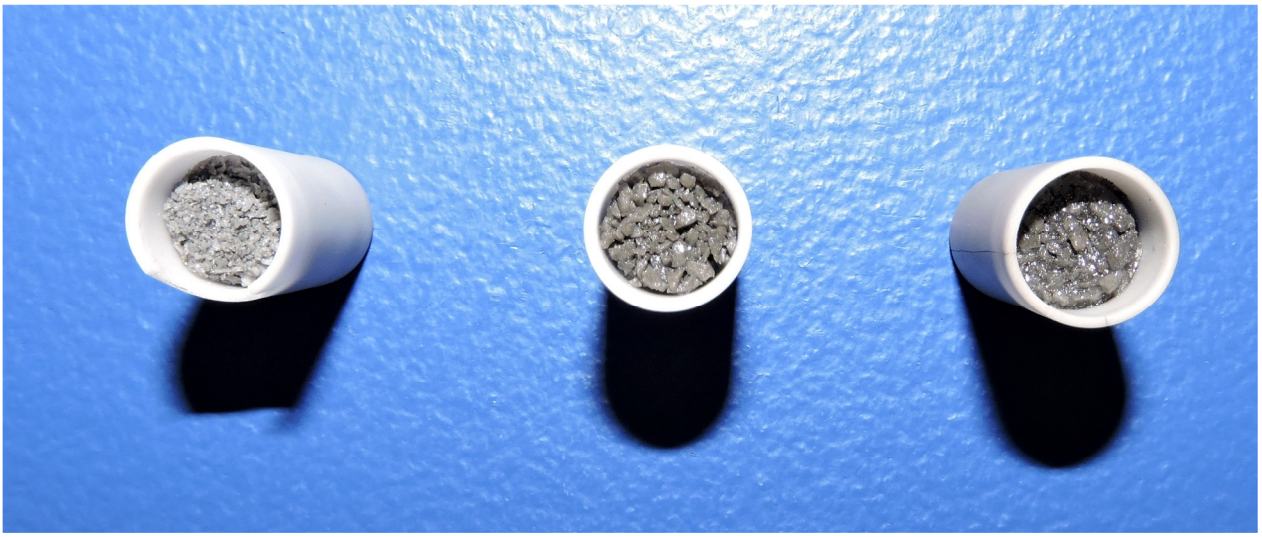

Figure B-5. Posttest Comparison of Melting Experiments on Rhyolite Samples at 1,320°C (Left), 1,400°C (Center), and 1,450°C (Right).

RSI-2492-15-031

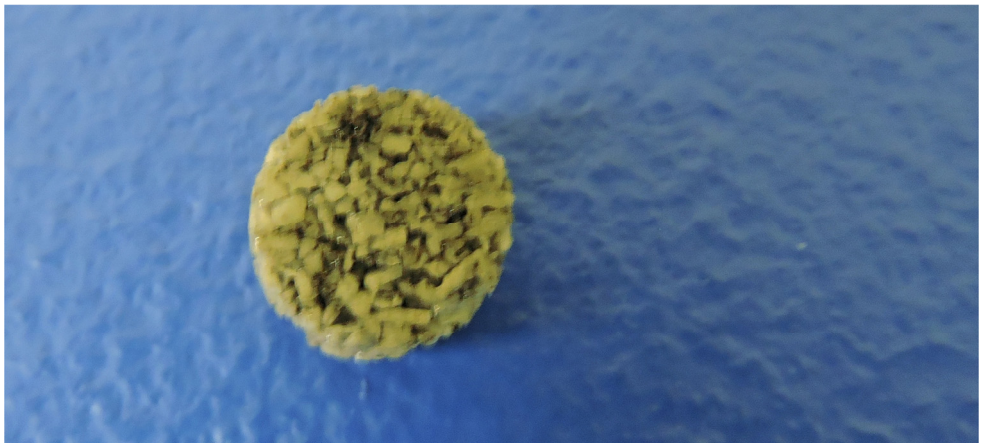

Figure B-6. Posttest Sample of Rhyolite After Being Heated to Temperature of 1,320°C.

RSI-2492-15-032

Figure B-7. Posttest Sample of Rhyolite After Being Heated to Temperature of 1,400°C.

RSI-2492-15-033

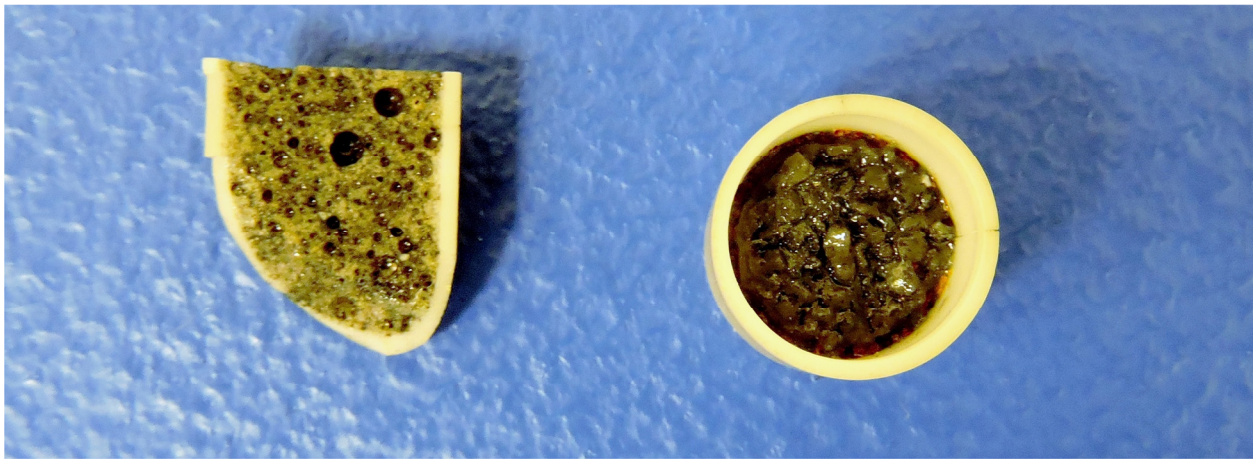

Figure B-8. Posttest Sample of Rhyolite After Being Heated to Temperature of 1,450°C.

Table B-6. Pre- and Postmelt Masses of Rhyolite Samples

Test	Temperature (°C)	Sample Mass		Mass Loss (%)
		Premelt (g)	Postmelt (g)	
Test 2	1,320	66.566	66.514	0.08
Test 3	1,400	66.944	66.819	0.19
Test 4	1,500	66.899	66.828	0.11
Test 5	1,450	66.268	66.210	0.09